Received: 5 January 2022 | Revised: 17 June 2022 | Accepted: 27 July 2022

DOI: 10.1002/oca.2934

RESEARCH ARTICLE

WILEY

A population model-based linear-quadratic Gaussian compensator for the control of intravenously infused alcohol studies and withdrawal symptom prophylaxis using transdermal sensing

Mengsha Yao[1] | **Susan E. Luczak**[2] | **Emily B. Saldich**[2] | **I. Gary Rosen**[3]

[1]Department of Mathematics, Temple University, Philadelphia, Pennsylvania, USA

[2]Department of Psychology, University of Southern California, Los Angeles, California, USA

[3]Department of Mathematics, University of Southern California, Los Angeles, CA, USA

Correspondence
I. Gary Rosen, Department of Mathematics, University of Southern California, Los Angeles, CA 90089, USA.
Email: grosen@math.usc.edu

Funding information
National Institute on Alcohol Abuse and Alcoholism/NIH, Grant/Award Numbers: R21AA017711, R01AA026368

Abstract

An output feedback linear-quadratic Gaussian compensator (combined controller and state estimator) for the regulation of intravenous-infused alcohol studies and treatment using a noninvasive transdermal alcohol biosensor is developed. The design is based on a population model involving an abstract semilinear parabolic hybrid reaction-diffusion system involving coupled partial and ordinary differential equations with random parameters known only up to their distributions. The scheme developed is based on a weak formulation of the model equations in an appropriately constructed Gelfand triple of Bochner spaces wherein the unknown random parameters are treated as additional spatial variables. Implementation relies on a Galerkin-based approximation and convergence theory and an abstract formulation involving linear semigroups of operators. The model is fit and validated using laboratory collected human subject data and the method of moments. The results of numerical simulations of controlled intravenous alcohol infusion are presented and discussed.

KEYWORDS

intravenously infused alcohol studies and therapy, LQG control and estimation in Hilbert space, model uncertainty, random abstract parabolic hybrid reaction-diffusion system, transdermal alcohol biosensor

1 | INTRODUCTION

The control problem of interest to us here involves the use of relatively newly developed transdermal alcohol concentration (TAC) biosensor technology to effect closed-loop feedback control of blood alcohol concentration (BAC) in response to an intravenously infused ethanol solution. The control objective is to have the patient's or study participant's BAC track a prespecified target trajectory typically in the form of a succession of prespecified constant levels. The need for such a control protocol arises, for example, in the in-patient clinical management of severe withdrawal symptoms in people suffering from alcohol use disorder (AUD),[1,2] and in both human and animal laboratory studies of the physiological effects

FIGURE 1 (Left) Giner, Inc. (Newton, Massachusetts) WristTAS™ 7 and (right) https://www.scramsystems.com/SCRAM Systems (Alcohol Monitoring Systems, Littleton Colorado) transdermal continuous alcohol monitoring devices

of the consumption of alcoholic beverages.[3,4] Our primary aim carrying out this research was to demonstrate the utility of this new technology beyond its simply serving as a replacement for the breathalyze and self report.

As early as the 1930's, researchers recognized that transdermal alcohol in perspiration is positively correlated with BAC.[5] Recently, research groups and commercial enterprises (established companies and start-ups) have exploited this observation and developed biosensors resembling a digital watch, a wearable personal fitness monitor, or an ankle bracelet (see Figure 1) that serve as abstinence monitors or provide TAC as a measure of intoxication.[6-9] However, other than the sensor itself being the focus of the study, researchers and clinicians have been reluctant to use them because TAC does not consistently map onto BAC or the most commonly used measure of alcohol intoxication, breath alcohol concentration, or BrAC. Breathalyzers have been shown to be stable across individuals and ambient environmental conditions.[10] Controlled experiments with TAC sensors, on the other hand, have shown that TAC is significantly affected by a number of confounding factors including physiological characteristics (e.g., skin thickness, porosity, tortuosity, blood flow, physical activity, level of perspiration/sweating, etc.), ambient environmental conditions (e.g., temperature, humidity), and the sensor hardware being worn. Thus, a method that could accurately and consistently estimate BAC or BrAC from TAC would be required before TAC could be used in the lab, clinic, or in the field.

Using a TAC biosensor to facilitate the automatic control of the treatment of AUD patients or of laboratory/clinical experiments designed to further the understanding of the physiological effects of alcohol would represent a significant advance. Indeed, the current protocols for inpatient intravenous alcohol therapies and clamping (i.e., involving a target BrAC trajectory that is constant) studies require either open-loop or manual titration of intravenously infused ethanol solutions. However, the very nature of the underlying system to be controlled and designing a controller to regulate it, pose a number of significant challenges. These include (1) the plant is bio- and electro-chemical in nature rather than mechanical, electronic, or digital, the more traditional domains of feedback control, (2) because the fundamental uncertainty in the system is associated with the dynamics of the TAC biosensor itself, and since there is no independent means to determine ground-truth while the process is evolving, adaptive methods are not a viable option, (3) there is no way to measure the effect of the controller input directly and in real time; in fact it is really the sensor dynamics that make this problem so difficult, and (4) the plant parameters are, in general, unknown, are patient-, environment-, and hardware-dependent, and are likely to vary while the treatment or experiment is in progress. The approach we develop here is intended to mitigate these obstacles.

Our research group consisting of applied mathematicians/control engineers, psychiatrists and psychologists has developed a number of techniques for estimating BAC or BrAC from observations of biosensor measured TAC based on either first principles physics-based models[11-13] or data-driven machine learning techniques such as physics informed artificial neural networks[14,15] and hidden Markov models.[16] In addition, several other research groups have developed standard regression models[17-19] and machine learning techniques such as random forest-like extra-trees[20] to convert TAC into either BAC or BrAC.

The earliest efforts to convert TAC into BAC or BrAC[11-13] required that the models be contemporaneously calibrated to each individual by collecting simultaneous BrAC and TAC data during a single drinking episode in the laboratory under controlled conditions. More recent treatments have eliminated the required calibration by replacing an individual model with what is known as a *population model*.[21-24] Rather than fitting model parameters to data from a single drinking episode, the model parameters are assumed to be random, and their distributions are fit to BrAC/TAC data from numerous drinking episodes from cohorts of individuals wearing different sensors and under various ambient conditions. These

population models are then used to estimate BAC or BrAC from TAC and provide a conservative error band without being individually calibrated.

In this article, we develop a method that uses (1) a TAC biosensor, (2) a semilinear, random reaction-diffusion, population model that describes the metabolism of alcohol in the liver, the transport of ethanol from the blood through the skin, and its measurement by the sensor, (3) linear-quadratic Gaussian (LQG) control and estimation for infinite-dimensional systems in Hilbert space, and (4) a new and novel way to deal with systems involving random parameters to automate the regulation of intravenously infused alcohol studies and therapies.

More specifically, our approach is a novel synthesis of a number of ideas and techniques that have been developed by various researchers and research groups including ours over the past four decades:

1. Our basic model for the transport of ethanol through the epidermal layer of the skin is a one-dimensional diffusion equation with input and output on the boundary of the spatial domain. This results in a state space formulation with unbounded input and output operators.[25,26] Consequently standard results for linear quadratic control (LQR/LQG) in Hilbert space are not directly applicable. In addition, the control problem of interest to us here requires a *full-body alcohol model* that also captures the enzyme catalyzed metabolism of ethanol in the liver and couples it with the transdermal transport through the epidermal layer.[12] We deal with these complications by relying on an idea from the product space-based state space formulation of hereditary or delay systems (see, e.g., References 27-30 and mechanical systems involving the transverse vibrations of flexible beams with tip bodies (see, e.g., References 31-34). The result is a semilinear abstract parabolic reaction-diffusion system of coupled ordinary and partial differential equations with bounded input and output operators.
2. To deal with the uncertainty (i.e., randomness) in the parameters appearing in the model, we design our combined LQG controller and observer, or LQG compensator, based on a state space formulation of a population model. To obtain this state space formulation, we take advantage of a relatively recently developed framework wherein abstract random parabolic systems are set in weak form in appropriately constructed Bochner spaces in which the random parameters are effectively treated as additional spatial variables.[35,36] Our group has used this general approach previously to fit forward models for the transdermal transport of ethanol with the primary goal being to solve the inverse problem of deconvolving BrAC input from TAC biosensor measurements.[21-23] However, other than our conference paper that briefly laid out some of these ideas in the continuous time case,[37] to the best of our knowledge, our treatment here is the first time anything like this has been used in the context of either open or closed loop control.
3. With the aforementioned state space formulation together with linear semigroup theory[38,39] and LQG control and estimation theory in infinite dimensional Hilbert spaces, the design of an output feedback compensator and convergence results for its finite-dimensional approximation become straightforward (References 40 and 41 for the continuous-time case and References 34 and 42 in the discrete or sampled time setting).

An outline of the remainder of this article is as follows. In Section 2, we provide a first-principle derivation of our semilinear hybrid ODE/PDE reaction-diffusion model and its linearization about steady state. In Section 3, we develop the state space formulation of our abstract parabolic system in terms of linear semigroups of operators, the extension of these ideas to the case where the equations involve random parameters, and we discuss their finite dimensional approximation and the associated convergence theory. Our LQG compensator and its finite dimensional approximation are presented in Section 4. In Section 5, we use human subject data collected in the Luczak lab at USC to fit and validate the individual and population models developed in Sections 2 and 3, and we validate our state estimator. In Section 6, we present our numerical simulation results demonstrating the efficacy of using our compensator to regulate the intravenous infusion of ethanol based on transdermal sensing. Finally, Section 7 has some discussion and concluding remarks.

2 | MODELING INTRAVENOUS ALCOHOL INFUSION WITH TRANSDERMAL SENSING

We consider the design of an output feedback LQG compensator or combined controller and state observer or estimator, for the purpose of regulating the intravenous infusion of ethanol with observations provided by a transdermal alcohol biosensor (see, e.g., References 3, 4, and 23). Our design is based on a pharmacokinetic/pharmacodynamic (PK/PD) compartment model that captures the intravenous infusion, metabolism, transdermal transport, and bio-sensor measurement

of ethanol. Since the primary challenge is the uncertainty and real-time variability (i.e., the randomness) in the model parameters, as will be explained below, our goal in constructing our state space model is to keep the number of parameters to an absolute minimum.

The conventional choice for describing with reasonable fidelity the movement of ethanol molecules through the skin would be a multi-compartment transport model. Instead, as in Reference 37, we rely on a one-dimensional diffusion equation. This approach offers a number of distinct advantages. Since the first principles empirical basis for the diffusion equation is Fick's law, the basic structure of the model captures the underlying physics and physiology of the transport process and consequently the number of unknown parameters is reduced. In addition, the coercivity of the diffusion operator forces both the open loop system and the closed loop compensator to be, intrinsically, highly stable.

On the other hand, the diffusion equation is a partial differential equation (PDE) and thus results in an infinite dimensional state space. However, the finite element approximation and associated convergence theory for the control and estimation of parabolic systems is straight forward and has been well studied for the last four decades. In particular, finite dimensional Galerkin approximation preserves coercivity and therefore the strong open and closed loop stability properties of the infinite dimensional system (see, e.g., References 34, 40, and 41). In addition, since the parameters associated with the skin compartment along with those associated with the dermal layer/blood and sensor compartments, are continuous, rather than discrete, random variables whose values are either known or fit only up to their distributions, they are also fundamentally infinite dimensional. Thus, dealing with them, one way or another, will also necessarily introduce infinite dimensionality into the state space formulation. Consequently, the decision to model the skin compartment using a PDE is essentially inconsequential and its benefits significantly out-weigh any potential disadvantages. Indeed, as we shall see in what follows, the complexity of our compensator is polynomial in the level of the state space discretization, but exponential in the number of random parameters that appear in the model. Therefore, we seek a model for which the dimension of the parameter space is as low as possible.

The epidermal layer of the skin sits atop the dermal layer. The dermal layer has an active blood supply while the epidermal layer does not. The latter consists of both dead (the stratum corneum layer, which is closest to the surface) and living (the deeper layers closer to the dermal layer) cells surrounded by interstitial fluid and blood plasma. Not having an active blood supply, the living cells in the epidermal layer obtain nourishment primarily from the interstitial fluid and O_2 that diffuses in from the environment beyond the skin.

The SCRAM TAC biosensor we use in our studies (see the right panel in Figure 1) has a perspiration vapor collection chamber on the bottom of the sensor that sits atop, and is in direct contact with, the stratum corneum layer of the skin's epidermal layer. Perspiration in vapor form collects in the chamber and from which a small pump extracts a sample of the vapor approximately once every 30 min. This sample is then electro-chemically analyzed based on an oxidation-reduction (redox) reaction in much the same way that a fuel cell produces a current (and heat and water) from hydrogen and oxygen. In the TAC sensor, ethanol molecules in the sample are oxidized, producing electrons in the form of an electrical current. This current is converted into the TAC measurement based on an a-priori bench calibration.

We note that by modeling the dermal layer of the skin, or equivalently the blood, and the TAC biosensor collection chamber as well-mixed compartments coupled to the diffusion equation for the epidermal layer at the boundaries, we are able to avoid having to deal with unbounded (see, e.g., References 25, 26, 42, and 43) input (i.e., actuator influence) and output (i.e., sensor influence) operators, thus greatly simplifying the mathematics underlying our design. The result is a SISO model that takes the form of a hybrid system of coupled ordinary and partial differential reaction-diffusion-transport equations with random coefficients.

2.1 | A model for intravenously infusing alcohol with transdermal sensing

Let Λ denote the thickness of the epidermal layer (units: cm) of the skin at the location of the TAC sensor and let $\tilde{\eta}$ denote the depth in the epidermal layer (units: cm), $0 \leq \tilde{\eta} \leq \Lambda$, $\tilde{\eta} = 0$ denoting the skin surface and $\tilde{\eta} = \Lambda$ denoting the boundary between the epidermal and dermal layers. Let t denote time (units: h) and let $\tilde{x}(t, \tilde{\eta})$ denote the concentration of ethanol at time t and depth $\tilde{\eta}$ in the epidermal layer (units: grams per milliliter of blood plasma). We note that the ethanol molecules are actually in what is known as the extracellular fluid which consists largely of blood plasma (the components of blood with the exception of the red blood cells) and interstitial fluid, a filtrate of blood plasma consisting of water, electrolytes

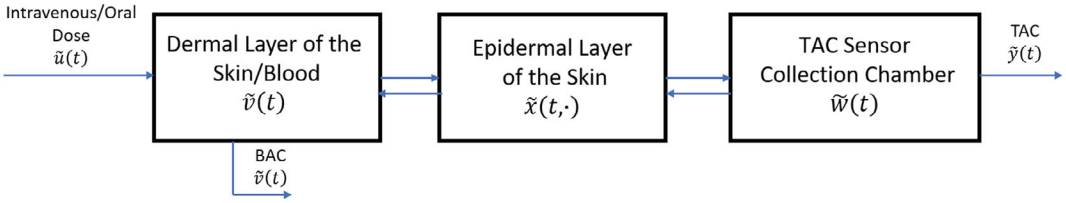

FIGURE 2 Signal flow diagram of the system given in Equation (1)

and other low mass solids which pass through selectively permeable capillary walls; for our purposes here, we shall simply assume that the ethanol is in suspension in the blood plasma. Let $\tilde{w}(t)$ denote the concentration of ethanol in the TAC sensor collection chamber at time t (units: grams per milliliter of air), let $\tilde{v}(t)$ denote the concentration of ethanol in the blood (or dermal layer of the skin) at time t (units: grams per milliliter of blood plasma) and let $\tilde{u}(t)$ denote the intravenous flow rate of ethanol solution at time t (our control or input, units: milliliters of ethanol solution per hour). Let $\tilde{y}(t)$ denote the TAC at time t (our observation or output, units: grams per milliliter of air), and let $\tilde{w}_0$ (units: grams per milliliter of air), $\tilde{v}_0$ (units: grams per milliliter of plasma) and φ_0 (units: grams per milliliter of interstitial fluid) denote the initial conditions for $\tilde{w}$, $\tilde{v}$, and $\tilde{x}$, respectively. Note that we assume that there is no ethanol in the blood, the dermal and epidermal layers of the skin, or the TAC biosensor collection chamber at time $t = 0$ so $\tilde{w}_0 = 0$, $\tilde{v}_0 = 0$, and $\varphi_0 = 0$. Letting T denote the duration of the study or therapy (units: h) and with these definitions, our model takes the form (see Figure 2)

$$
\begin{aligned}
\frac{\partial \tilde{x}}{\partial t}(t,\tilde{\eta}) &= \alpha \frac{\partial^2 \tilde{x}}{\partial \tilde{\eta}^2}(t,\tilde{\eta}), \quad 0 < \tilde{\eta} < \Lambda, \quad 0 < t < T,\\
\frac{d\tilde{w}}{dt}(t) &= \frac{\gamma\alpha}{\rho_{P/A}} \frac{\partial \tilde{x}}{\partial \tilde{\eta}}(t,0) - \delta \tilde{w}(t), \quad 0 < t < T,\\
\frac{d\tilde{v}}{dt}(t) &= -\zeta\alpha \frac{\partial \tilde{x}}{\partial \tilde{\eta}}(t,\Lambda) - \epsilon \tilde{v}(t) - \frac{V_{\max}\tilde{v}(t)}{K_{\mathrm{M}} + \tilde{v}(t)} + \frac{\xi \rho_{W/P}}{\beta}\tilde{u}(t), \quad 0 < t < T,\\
\tilde{y}(t) &= \theta \tilde{w}(t), \quad 0 < t < T,\\
\tilde{x}(t,0) &= \rho_{P/A}\tilde{w}(t), \quad \tilde{x}(t,\Lambda) = \tilde{v}(t), \quad 0 < t < T,\\
\tilde{w}(0) &= \tilde{w}_0, \quad \tilde{v}(0) = \tilde{v}_0, \ \tilde{x}(0,\tilde{\eta}) = \varphi_0(\tilde{\eta}), \ 0 < \tilde{\eta} < \Lambda,
\end{aligned}
\tag{1}
$$

where $\alpha > 0$ denotes the *effective* diffusivity of ethanol in the blood plasma in the epidermal layer (units: cm^2/h), $\rho_{P/A}$ and $\rho_{W/P}$ denote respectively, the partition coefficients for ethanol in plasma and air, and water and plasma, with respect to the concentration units of grams per milliliter of water, grams per milliliter of plasma, and grams per milliliter of air at 37°C (normal body temperature). Based on an empirical relationship from physical chemistry known as Henry's law, when a liquid is in contact with a gas, the concentrations, C_L and C_G, of a molecule present in both the liquid and the gas will come to equilibrium according to the linear relationship $C_L = \rho_{L/G}C_G$, where the constant $\rho_{L/G}$, known as the partition coefficient, is temperature dependent and depends on the compound, the liquid, and the gas. Its numerical value will vary depending on the choice of units for C_L and C_G. It has been shown (see, e.g., Reference 44) that at 34°C, the partition coefficient for ethanol in blood and air is $\rho_{B/A} = 2157 \pm 9.6$ for men and $\rho_{B/A} = 2195 \pm 10.9$ for women, at 37°C, the partition coefficient for ethanol in blood and air is $\rho_{B/A} = 1783 \pm 8.1$ for men and $\rho_{B/A} = 1830 \pm 7.8$ for women. Using a regression model, Jones[44] found that at 37°C the partition coefficient for ethanol in water and air is $\rho_{W/A} = 2133$, in blood and air is $\rho_{B/A} = 1756$, and between plasma (all of the components of blood with the exception of the oxygen carrying red blood cells) and air it is $\rho_{P/A} = 2022$. All of these values are for the case when the concentration of ethanol in air is given in units of grams per liter, and in water, blood, or plasma in units of grams per deciliter. We note that it is generally accepted that a BrAC reading of 0.08 percent alcohol corresponds to 0.008 grams of ethanol per 210 liters of breath and a BAC of 0.08 grams of ethanol per 100 milliliters (equal to 1 deciliter (dL) or 0.1 liters (L)) of blood.

In modeling the TAC collection chamber (dermal layer or blood) as a well-mixed compartment, we assume that the inflow (outflow) of ethanol is proportional to the flux out of (i.e., from right to left) (into (i.e., from left to right)) the epidermal layer at the surface of the skin (i.e., at $\tilde{\eta} = 0$) (the boundary of the epidermal and dermal layers of the skin

(i.e., at $\tilde{\eta} = \Lambda$)), $\alpha \frac{\partial \tilde{x}}{\partial \tilde{\eta}}(t, 0)$ ($-\alpha \frac{\partial \tilde{x}}{\partial \tilde{\eta}}(t, \Lambda)$), with constants of proportionality γ (units: cm^{-1}) (ζ (units: cm^{-1})), and the linear outflow in both cases is simply proportional to the concentration of ethanol in the collection chamber (dermal layer or blood) with constant of proportionality δ (units: h^{-1}) (ϵ (units: h^{-1})). In the input gain, ξ is the concentration of the ethanol solution (units: grams of ethanol per milliliter of solution) and β is the volume of blood plasma in the body (units: milliliters).

In the SCRAM TAC biosensor, the ethanol sample is processed as a reactant in an oxidation-reduction reaction wherein molecules of ethanol are oxidized producing electrons which are then counted in the form of an electrical current. This measured current is then bench calibrated with a source of ethanol vapor with known concentration. In the system (1), the output gain, θ, represents the bench calibration factor for the TAC sensor that converts the concentration of ethanol in the collection chamber into TAC (units: dimensionless).

With regard to the reaction term in the equation for the ethanol concentration in the blood compartment, aside from the relatively small amount of ethanol excreted from the body through urine, tears, breast milk, sweat, and perspiration, the primary mechanism by which ethanol is processed out of the body is via an enzyme-catalyzed chemical reaction that takes place in the liver. This group of enzymes is known as alcohol dehydrogenase (ADH). As is standard for enzyme-catalyzed reactions, we model this metabolic process with a Michaelis–Menten term which exhibits first-order kinetics at low concentrations and zero-order kinetics at higher concentrations once enzyme saturation is achieved. The dynamics are described via two parameters, $V_{\max}$, the maximum reaction rate achieved at the saturating ethanol concentration (units: grams per milliliter of blood plasma per hour), and K_{M}, known as the Michaelis constant (units: grams per milliliter of blood plasma), the ethanol concentration when the reaction rate is $\frac{1}{2}V_{\max}$.

In the system (1), the only parameters for which either in vitro or in vivo empirically determined values can be found in the literature are the partition coefficients for ethanol (see, e.g., Reference 44), the thickness of the epidermal layer, Λ, and the Michaelis–Menten constants, $V_{\max}$ and K_{M} (see, e.g., Reference 45). Consequently, the values of the parameters in (1), which we would expect to vary across individual subjects, sensors, and possibly ambient environmental conditions (e.g., temperature, humidity, etc.), will have to be estimated computationally from input/output data. Since Λ determines the spatial domain of the diffusion equation, it is mathematically and computationally challenging to estimate. In light of this, we make the change of variables $\eta = \frac{\tilde{\eta}}{\Lambda}$, $\hat{x}(t, \eta) = \tilde{x}(t, \eta\Lambda)$, $\hat{w}(t) = \rho_{P/A}\tilde{w}(t)$, $\hat{v}(t) = \tilde{v}(t)$, $\hat{u}(t) = \tilde{u}(t)$, and $\hat{y}(t) = \frac{\rho_{P/A}}{\theta}\tilde{y}(t)$, and obtain the transformed hybrid reaction-diffusion-transport, input/output system given by

$$
\begin{aligned}
\frac{\partial \hat{x}}{\partial t}(t, \eta) &= q_1 \frac{\partial^2 \hat{x}}{\partial \eta^2}(t, \eta), \quad 0 < \eta < 1, \quad 0 < t < T, \\
\frac{d\hat{w}}{dt}(t) &= q_3 \frac{\partial \hat{x}}{\partial \eta}(t, 0) - q_4 \hat{w}(t), \quad 0 < t < T, \\
\frac{d\hat{v}}{dt}(t) &= -q_5 \frac{\partial \hat{x}}{\partial \eta}(t, 1) - q_6 \hat{v}(t) - \frac{q_7 \hat{v}(t)}{q_8 + \hat{v}(t)} + q_2 \hat{u}(t), \quad 0 < t < T, \\
\hat{y}(t) &= \hat{w}(t), \quad 0 < t < T, \\
\hat{x}(t, 0) &= \hat{w}(t), \quad \hat{x}(t, 1) = \hat{v}(t), \quad 0 < t < T, \\
\hat{w}(0) &= 0, \quad \hat{v}(0) = 0, \ \hat{x}(0, \eta) = 0, \ 0 < \eta < 1,
\end{aligned} \tag{2}
$$

where $q_1 = \frac{\alpha}{\Lambda^2}$, $q_2 = \frac{\xi \rho_{W/P}}{\beta}$, $q_3 = \frac{\gamma\alpha}{\Lambda}$, $q_4 = \delta$, $q_5 = \frac{\zeta\alpha}{\Lambda}$, $q_6 = \epsilon$, $q_7 = V_{\max}$, and $q_8 = K_{\text{M}}$, with $q_i \geq 0$, $i = 1, 2, \ldots, 8$.

2.2 | Linearization about steady state

Our compensator is designed to regulate about the steady state or equilibrium solution to (2). A desired clamping BAC level, $\hat{v}(t) = \hat{v}^0, 0 \leq t \leq T$ is specified, and then based on it, the steady state solution $\hat{x}_0(\eta) = \frac{\hat{v}^0(q_4\eta + q_3)}{q_3 + q_4}, 0 \leq \eta \leq 1, \hat{w}_0 = \frac{q_3\hat{v}^0}{q_3+q_4}$, $\hat{v}_0 = \hat{v}^0$, $\hat{u}_0 = \frac{q_5q_4 + q_6(q_3+q_4)}{q_2(q_3+q_4)}\hat{v}^0 + \frac{q_7}{q_2(q_8+\hat{v}^0)}\hat{v}^0$, $\hat{y}_0 = \frac{q_3\hat{v}^0}{q_3+q_4}$ can be computed. We then set $\hat{x} = \hat{x}_0 + x$, $\hat{w} = \hat{w}_0 + w$, $\hat{v} = \hat{v}_0 + v$, $\hat{u} = \hat{u}_0 + u$, and $\hat{y} = \hat{y}_0 + y$ and obtain the linearized system for x, w, v, u, and y given by:

$$\begin{aligned}\frac{\partial x}{\partial t}(t,\eta) &= q_1\frac{\partial^2 x}{\partial \eta^2}(t,\eta), \quad t>0, \quad \eta\in(0,1),\\ \frac{dw}{dt}(t) &= q_3\frac{\partial x}{\partial \eta}(t,0) - q_4 w(t) + \omega_1(t), \quad t>0,\\ \frac{dv}{dt}(t) &= -q_5\frac{\partial x}{\partial \eta}(t,1) - (q_6+q_L)v(t) + q_2 u(t) + \omega_2(t), \quad t>0,\end{aligned} \tag{3}$$

with boundary conditions, controlled variable and observation:

$$x(t,0) = w(t), \quad x(t,1) = v(t), \quad z(t) = v(t), \quad y(t) = w(t) + \zeta(t), \quad t>0, \tag{4}$$

respectively, where in the system (3), (4), the parameter $q_L = \frac{V_{\max}K_M}{(K_M+\hat{v}^0)^2} = \frac{q_7 q_8}{(q_8+\hat{v}^0)^2}$, and ω_1, ω_2, and ζ denote uncorrelated, zero-mean, stationary, Gaussian white noise processes with variances σ_1^2, σ_2^2, and σ^2. It is also possible to include random noise in the diffusion equation using one of the available treatments of stochastic processes in infinite-dimensional space (see, e.g., References 46 and 47). However, in the interest of clarity, since this is not the central focus of this research, we have decided to omit this.

The state of the system (3), (4) is given by the triple (w,v,x), the quantity to be controlled by $z=v$, the output by y, and the input by u. The objective is to design an output feedback law for u that is a function of $y=\hat{y}-y_0$ so that when the system (2) experiences a disturbance, the input $\hat{u}=\hat{u}_0+u$ will drive v to zero and then maintain it there while also staying within the bounds required for the safety of the patient or study participant. The challenge of course is to do this in the case where a subset of the model parameters, $q=[q_1,q_2,q_3,q_4,q_5,q_6,q_7,q_8]$, are known only up to their distribution in a cohort population of interest.

It is clear from the preceding paragraph that our compensator will depend on the values for the steady state input or *maintenance dose*, $\hat{u}_0$, and the steady state output, $\hat{y}_0$, which in turn depend on the unknown parameters, q. A *loading dose*, $\hat{u}^0$, will also be required to safely and efficiently bring the patient/participant up to the desired clamped BAC level, $\hat{v}_0$. We note however, that the loading and maintenance doses, $\hat{u}^0$ and $\hat{u}_0$, respectively, can be computed independently from the model[3,4,48] either empirically, or based on a statistical regression model with predictor variables derived from readily observable or computable covariates such as total body water, weight, height, age, sex, and so forth.[49] The corresponding steady state TAC value, $\hat{y}_0$, can then be obtained directly from the sensor once the BAC or BrAC stabilizes or from a-priori calibration curves for the particular sensor being used.

3 | THE STATE SPACE FORMULATION OF THE INDIVIDUAL AND POPULATION MODELS

3.1 | Abstract parabolic systems and the individual models

Let V and H be Hilbert spaces with $V \hookrightarrow H$, that is, V is continuously and densely embedded in H. Then the Gelfand triple $V \hookrightarrow H \hookrightarrow V^*$ is obtained by identifying H with its dual H^*. Define the inner product on H by $\langle\cdot,\cdot\rangle_H$ and the norms on H and V by $|\cdot|_H$, $\|\cdot\|_V$, respectively. Define a sesquilinear form $a(\cdot,\cdot): V\times V\to\mathbb{C}$ which satisfies the following properties:

Assumption 1 (Boundedness). There exists a constant $\alpha_0>0$ such that for each $\varphi,\psi\in V$, we have $|a(\varphi,\psi)|\le \alpha_0\|\varphi\|_V\|\psi\|_V$.

Assumption 2 (Coercivity). There exist constants $\lambda_0\in\mathbb{R}$ and $\mu_0>0$ such that for each $\varphi\in V$, we have $a(\varphi,\varphi)+\lambda_0|\varphi|_H^2\ge\mu_0\|\varphi\|_V^2$.

We consider the parabolic system in weak form:

$$\langle\dot{x},\psi\rangle_{V^*,V} + a(x,\psi) = \langle Bu,\psi\rangle_{V^*,V}, \psi\in V, x(0)=x_0, \tag{5}$$

where $x_0\in H$, $u\in L^2([0,T],U)$ is an input to the system, and either $B: U\to V^*$ or $B: U\to H$ is a bounded linear operator.

It can be shown that (5) has a unique solution in the set:

$$\left\{\psi : \psi \in L^2([0,T],V), \dot{\psi} \in L^2([0,T],V^*)\right\} \subseteq C([0,T],H).$$

Under these assumptions, $a(\cdot,\cdot)$ defines a bounded linear operator $A : V \to V^*$ such that $-a(\varphi,\psi) = \langle A\varphi,\psi\rangle_{V^*,V}$ where $\varphi,\psi \in V$. Furthermore, it can be shown[39,43] that A, restricted to the set $\mathrm{Dom}(A) = \{\varphi \in V : A\varphi \in H\}$, is the infinitesimal generator of a holomorphic or analytic semigroup of bounded linear operators on H, $\{T(t) : t \geq 0\}$. Moreover, this semigroup can be restricted to be a holomorphic semigroup on V and extended to be a holomorphic semigroup on V^* by appropriately restricting or extending the domain, $\mathrm{Dom}(A)$, of the operator A (see, e.g., References 39 and 43).

It follows that the system (5) can be rewritten in state space form as the evolution system with time-invariant operators A and B:

$$\dot{x}(t) = Ax(t) + Bu(t), \quad x(0) = x_0. \tag{6}$$

Using the semigroup, the unique mild solution to the (6) is given by

$$x(t) = T(t)x_0 + \int_0^t T(t-s)Bu(s)ds, \quad t \geq 0.$$

In addition, a semilinear system such as the one given in (1) or (2) can also be written in state space form. For example, if $F : [0,\infty) \times H \to H$ denotes a nonlinear perturbation, the state space model would now be given by

$$\dot{x}(t) = Ax(t) + F(t,x(t)) + Bu(t), \quad x(0) = x_0. \tag{7}$$

Existence, uniqueness, and regularity results for abstract semilinear systems like the one given in (7) in which the operator A is the infinitesimal generator of either a C_0, analytic, or compact semigroup can be found in Reference 38. The compact case does not apply here since our state space is infinite dimensional. Although our operator A does generate a holomorphic, or analytic semigroup, the results in Reference 38 for semilinear equations with C_0 semigroups are more than adequate for our purposes here. Indeed, if u and F are continuous in t and F is uniformly Lipschitz on H (i.e., there exists an $L > 0$ such that $|F(t,\varphi) - F(t,\psi)|_H \leq |\varphi - \psi|_H$, $\varphi,\psi \in H$) then the semilinear abstract evolution Equation (7) admits a unique mild solution; that is a continuous solution to the integral equation in H given by the expression in (8) below as

$$x(t) = T(t)x_0 + \int_0^t T(t-s)\{F(s,x(s)) + Bu(s)\}ds. \tag{8}$$

If in addition, u and F are Lipschitz continuous in t as well, and $x_0 \in \mathrm{Dom}(A)$, then the mild solution is a strong solution, and if Bu and F are continuously differentiable from $[0,T] \times H$ into H with $x_0 \in \mathrm{Dom}(A)$, then x, the unique solution to the integral equation (8), is a classical solution to (7).

3.2 | Random parameters as auxiliary spatial variables and the population models

We summarize the key idea from the framework developed in References 21-23, 35, and 36, and consider an abstract parabolic system with random parameters satisfying a known (either given or fit) distribution.

Assume $q \in Q$, where the admissible parameter set, Q, is a compact (with respect to some metric, d_Q) subset of the finite-dimensional Euclidean space whose dimension is p. For each $q \in Q$, we require that besides satisfying Assumptions 1 and 2, the form $a(q;\cdot,\cdot) : V \times V \to \mathbb{C}$ also satisfies:

Assumption 3 (Continuity). For $q,\tilde{q} \in Q$, we have for all $\varphi,\psi \in V$, $|a(q;\varphi,\psi) - a(\tilde{q};\varphi,\psi)| \leq d_Q(q,\tilde{q})\|\varphi\|_V\|\psi\|_V$, where $d_Q(\cdot,\cdot)$ denotes any p-metric on $\mathbb{R}^p$.

At this point we assume further that the constants in Assumptions 1 and 2, α_0, λ_0, and μ_0, do not depend on $q \in Q$. In addition it may also sometimes be required that the inner product on the space H depends upon $q \in Q$. Let this space be denoted by $H_q = \{H, \langle \cdot, \cdot \rangle_q, |\cdot|_q\}$ and that the following assumption be satisfied.

Assumption 4 (H-continuity). For $q, \tilde{q} \in Q$, we have for all $\varphi, \psi \in H$, $|\langle \varphi, \psi \rangle_q - \langle \varphi, \psi \rangle_{\tilde{q}}| \leq d_Q(q, \tilde{q})|\varphi|_H|\psi|_H$, and that the identity map from V into H_q be uniformly bounded for $q \in Q$.

We formulate a population model by treating the parameter q as a random vector $\mathscr{q}$, with support given by the set of admissible parameters Q assumed to be a compact subset of Euclidean space, $\mathbb{R}^8$. We note that in practice, it is often convenient to assume either independent or dependent standard distributions for the q_i's (e.g., Normal, Gamma, Beta, etc.) whose supports are not necessarily compact and whose distributions depend on parameters in some parameter set $\Theta \subset \mathbb{R}^r$, for some r which we do assume is closed and bounded. We note that if one of these standard distributions is chosen, some aspects of our underlying mathematical theory may require, at least formally, for example, that their supports be considered to be truncated to a closed and bounded subset of $\mathbb{R}^8$, or that their supports do not contain the origin, or that certain moments (positive and negative) exist. Our experience has shown that in most applications of interest, these additional assumptions are of no practical concern. We assume that the distribution of $\mathscr{q}$ is given by either a known or fit measure $\pi = \pi(\theta)$, with $\theta \in \Theta$. It will typically be the case that the population model is determined by fitting the parameters θ to population data (see, e.g., References 21-23 and 50) as we will explain in somewhat greater detail and provide examples of below.

Define the Bochner spaces $\mathcal{V} = L^2_\pi(Q; V)$, $\mathcal{H} = L^2_\pi(Q; H_q)$ corresponding to the measure π. Then the assumptions on the spaces V and H guarantee that the spaces $\mathcal{V}$, $\mathcal{H}$ and $\mathcal{V}^*$ form the Gelfand triple $\mathcal{V} \hookrightarrow \mathcal{H} \hookrightarrow \mathcal{V}^*$ (see Reference 35). Here $\mathcal{H}$ has been identified with its dual $\mathcal{H}^* = L^2_\pi(Q; H^*_q)$ (see References 35 and 36).

We define the sesquilinear form $\mathscr{a}(\cdot, \cdot) : \mathcal{V} \times \mathcal{V} \to \mathbb{C}$ by

$$\mathscr{a}(\varphi, \psi) = \int_Q a(q; \varphi(q), \psi(q)) d\pi(q) = \mathbb{E}_\pi[a(q; \varphi(q), \psi(q))], \tag{9}$$

where $\varphi, \psi \in \mathcal{V}$. Assumptions 1–3 guarantee that this integral is well defined on q. The boundedness and coercivity of $\mathscr{a}(\cdot, \cdot)$ follow from Assumptions 1–3, and Cauchy–Schwartz. Therefore, we can use this sesquilinear form to define a bounded linear map $\mathcal{A} : \mathcal{V} \to \mathcal{V}^*$ by

$$\langle \mathcal{A}\varphi, \psi \rangle_{\mathcal{V}^*, \mathcal{V}} = -\mathscr{a}(\varphi, \psi), \quad \varphi, \psi \in \mathcal{V}, \tag{10}$$

which when appropriately restricted or extended is the infinitesimal generator of analytic semigroups of bounded linear operators $\mathcal{T}(t)$, $t \geq 0$ on $\mathcal{V}$, $\mathcal{H}$, and $\mathcal{V}^*$.

We next consider a nonhomogeneous parabolic system with random parameters written in the weak form:

$$\langle \dot{x}, \psi \rangle_{V^*, V} + a(q; x, \psi) = \langle B(q)u, \psi \rangle_{V^*, V}, \quad \psi \in V, \tag{11}$$

where $B(q) : U \to V^*$ (or $B(q) : U \to H$) is a bounded linear operator defined on a Hilbert space of feasible inputs, U, and $u \in L^2([0, \infty), L^2_\pi(Q; U))$. Then let $\mathcal{U}$ be a closed subspace of the Bochner space $L^2_\pi(Q; U)$ and define the operator $\mathcal{B} : \mathcal{U} \to \mathcal{V}^*$ by

$$\langle \mathcal{B}u, \psi \rangle_{\mathcal{V}^*, \mathcal{V}} = \int_Q \langle B(q)u(q), \psi(q) \rangle_{V^*, V} d\pi(q), \tag{12}$$

where $u \in \mathcal{U}$, $\psi \in \mathcal{V}$. In light of (9) and (12), as in the deterministic case, we can write the population model corresponding to (11) in weak (with respect to both $\eta \in (0, 1)$ and $q \in Q$) form as

$$\langle \dot{x}, \psi \rangle_{\mathcal{V}^*, \mathcal{V}} + \mathscr{a}(x, \psi) = \langle \mathcal{B}u, \psi \rangle_{\mathcal{V}^*, \mathcal{V}}, \quad \psi \in \mathcal{V}, \tag{13}$$

and then, using (10) and (12), in state space form as

$$\dot{x}(t) = \mathcal{A}x(t) + \mathcal{B}u(t), \quad x(0) = x_0, \tag{14}$$

where $u \in L^2([0,\infty), \mathcal{U})$. It is shown in References 35 and 36 that the solutions to (11) and (13) (or equivalently (14)) agree almost surely or $\pi - a.e \quad q \in Q$. It is interesting to note that in this way, the random parameters are effectively treated as additional spatial variables and, in particular, that the resulting weak form does not involve any derivatives with respect to these variables. More to the point, the resulting dynamical system (14) is now effectively deterministic and abstract parabolic and thus amenable to the treatment for standard abstract parabolic systems discussed previously in Section 3.1.

From semigroup theory,[39] the mild solution of (14) is

$$x(t) = \mathcal{T}(t)x_0 + \int_0^t \mathcal{T}(t-s)\mathcal{B}u(s)ds, \quad t \geq 0. \tag{15}$$

In the semilinear case, let $\mathcal{F} : [0,\infty) \times \mathcal{H} \to \mathcal{V}^*$ by

$$\langle \mathcal{F}(t,x), \psi \rangle_{\mathcal{V}^*,\mathcal{V}} = \int_Q \langle F(t, x(q), q), \psi(q) \rangle_{V^*,V} d\pi(q).$$

Once again, under appropriate assumptions, the results in Reference 38 for semilinear equations involving C_0 semigroups discussed previously, yield a unique mild, strong, or classical solution to the semilinear evolution equation in $\mathcal{H}$ given by

$$\dot{x}(t) = \mathcal{A}x(t) + \mathcal{F}(t, x(t)) + \mathcal{B}u(t), \;\; x(0) = x_0 \tag{16}$$

in the form of the solution to the integral equation in $\mathcal{H}$ given by

$$x(t) = \mathcal{T}(t)x_0 + \int_0^t \mathcal{T}(t-s)\{\mathcal{F}(s, x(s)) + \mathcal{B}u(s)\}ds. \tag{17}$$

Let τ denote the length of the sampling interval, and consider zero-order hold inputs of the form $u(t) = u_k$, for $t \in [k\tau, (k+1)\tau)$, $k = 0, 1, 2, \ldots$. If we then define $x_k = x(k\tau)$, $k = 0, 1, 2, \ldots$ and $\hat{\mathcal{A}} \in \mathcal{L}(\mathcal{V}, \mathcal{V})$, $\hat{\mathcal{B}} \in \mathcal{L}(\mathcal{U}, \mathcal{V})$ respectively by $\hat{\mathcal{A}} = \mathcal{T}(\tau)$ and $\hat{\mathcal{B}} = \int_0^\tau \mathcal{T}(s)\mathcal{B}ds$, we obtain the discrete-time dynamical system corresponding to (14) and (15) given by:

$$x_{k+1} = \hat{\mathcal{A}}x_k + \hat{\mathcal{B}}u_k, \quad x(0) = x_0. \tag{18}$$

We note that if the operator $\mathcal{A}$ given in (10) is invertible (e.g., if $\lambda_0 = 0$ in Assumption 2), it follows that $\hat{\mathcal{B}} = \int_0^\tau \mathcal{T}(s)\mathcal{B}ds = (\hat{\mathcal{A}} - I)\mathcal{A}^{-1}\mathcal{B} = \mathcal{A}^{-1}(\hat{\mathcal{A}} - I)\mathcal{B}$.

In the semilinear case, for $k = 0, 1, 2, \ldots$, we define $\tilde{\mathcal{F}}_k : \mathcal{H} \to \mathcal{H}$ by $\tilde{\mathcal{F}}_k(x) = \int_0^\tau \mathcal{T}(s)\mathcal{F}(k\tau, x)ds = (\hat{\mathcal{A}} - I)\mathcal{A}^{-1}\mathcal{F}(k\tau, x) = \mathcal{A}^{-1}(\hat{\mathcal{A}} - I)\mathcal{F}(k\tau, x)$. Then from (16) and (17), the semilinear discrete-time evolution system is given by

$$x_{k+1} = \hat{\mathcal{A}}x_k + \tilde{\mathcal{F}}_k(x_k) + \hat{\mathcal{B}}u_k \quad x(0) = x_0. \tag{19}$$

Finally we note that if there is an output or observation operator and/or a controlled variable operator, respectively, $C(q) \in \mathcal{L}(H_q, Y)$ (or $L(V, Y)$), where Y denotes the observation Hilbert space, and $D(q) \in \mathcal{L}(H_q, Z)$ (or $L(V, Z)$), where Z denotes the controlled variable Hilbert space, let $\mathcal{Y} = Y$ and $\mathcal{Z} = Z$ and define $\hat{\mathcal{C}} \in \mathcal{L}(\mathcal{H}, \mathcal{Y})$ (or $\mathcal{L}(\mathcal{V}, \mathcal{Y})$) and $\hat{\mathcal{D}} \in \mathcal{L}(\mathcal{H}, \mathcal{Z})$ (or $\mathcal{L}(\mathcal{V}, \mathcal{Z})$) by $\hat{\mathcal{C}}v = \int_Q C(q)v(q)d\pi(q)$ and $\hat{\mathcal{D}}v = \int_Q D(q)v(q)d\pi(q)$, respectively. Then the system (18) or (19) can be augmented with the output and controlled variable equations

$$y_k = \hat{\mathcal{C}}x_k, \quad z_k = \hat{\mathcal{D}}x_k, \quad k = 0, 1, 2, \ldots, \tag{20}$$

respectively. We note that once the appropriate identifications are made and the operators $A = A(q)$, $B = B(q)$, $C = C(q)$, $D = D(q)$, $\mathcal{A}$, $\mathcal{B}$, $\mathcal{C}$, and $\mathcal{D}$ and the functions $F_k(q)$ and $\mathcal{F}_k$ introduced in Sections 3.1 and 3.2 are appropriately defined

based on the systems (2) and (3), (4), the resulting systems (6) and (7) are referred to as the *individual models* and the systems (18), (20) and (19), (20) as the *population models*.

3.3 | Finite-dimensional approximation and convergence

We consider Galerkin approximations based on the weak form (13) (see Reference 40 for details). Arguing the convergence of approximating solutions to the population models in the form of the nonhomogeneous and semilinear equations, (18) and (19), respectively (and the strong convergence of the operators that appear in them as a requisite for convergence of the closed loop solutions to the finite dimensional approximating control and estimation problems to be considered below), is straight forward once one has established the strong convergence of the finite dimensional approximations to the semigroup (see, e.g., References 12, 13, 21, 34, 40, 42, 43, and 51). Consequently, here we focus on the convergence of approximations to the semigroup of operators on $\mathcal{H}$, $\{\mathcal{T}(t) : t \geq 0\}$.

Let N be a positive integer. For each N, let $\mathcal{V}^N$ be a finite-dimensional subspace of $\mathcal{V}$, satisfying $\mathcal{P}^N x \to x$, for $x \in \mathcal{V}$, where $\mathcal{P}^N$ is the orthogonal projection of $\mathcal{V}$ onto $\mathcal{V}^N$. Now we define the operators $\mathcal{A}^N$ on $\mathcal{V}^N$ by essentially restricting the form $\mathscr{a}$ to the subspace $\mathcal{V}^N \times \mathcal{V}^N$ of the space $\mathcal{V} \times \mathcal{V}$. To be more specific, we have for $\varphi^N, \psi^N \in \mathcal{V}^N$

$$\langle \mathcal{A}^N \varphi^N, \psi^N \rangle_{\mathcal{V}^N,\ \mathcal{V}^N} = -\mathscr{a}(\varphi^N, \psi^N) = -\int_Q a(q; \varphi^N(q), \psi^N(q)) d\pi(q).$$

Obviously, since $\mathcal{A}^N$ is a linear operator on a finite-dimensional space, it is the infinitesimal generator of a uniformly continuous semigroup $\mathcal{T}^N(t) = e^{\mathcal{A}^N t}$ for $t \geq 0$. So we can define $\hat{\mathcal{A}}^N \in \mathcal{L}(\mathcal{V}^N, \mathcal{V}^N)$ by $\hat{\mathcal{A}}^N = \mathcal{T}^N(\tau) = e^{\mathcal{A}^N \tau}$.

We use a variational corollary of Trotter–Kato theorem (see Theorems 2.1, 2.2, and 2.3 in Reference 52) to obtain the convergence of the approximating semigroups, and thereby, we obtain the convergence of the operators $\hat{\mathcal{A}}^N$.

Theorem 1. *Assume that the Assumptions 1–3 are satisfied. Then for each $x \in \mathcal{V}$, $\mathcal{T}^N(t)\mathcal{P}^N x \to \mathcal{T}(t)x$ in the $\mathcal{V}$ norm for $t > 0$, uniformly in t on compact sub intervals.*

The Trotter–Kato theorem (see Reference 52) requires the following assumption: For each $x \in \mathcal{V}$, there exists $x^N \in \mathcal{V}^N$ such that $\|x - x^N\|_{\mathcal{V}} \to 0$. However, we note that this assumption is actually equivalent to the strong convergence of the orthogonal projection $\mathcal{P}^N$ of $\mathcal{V}$ onto $\mathcal{V}^N$, that is, for any $x \in \mathcal{V}$, $\mathcal{P}^N x \to x$ as $N \to \infty$. Indeed, for any $x \in \mathcal{V}$ satisfying the assumption in Reference 52, we have $\|\mathcal{P}^N x - x\|_{\mathcal{V}} \leq \|x - x^N\|_{\mathcal{V}} \to 0$. On the other hand, for any $x \in \mathcal{V}$ satisfying $\mathcal{P}^N x \to x$ as $N \to \infty$, take $x^N = \mathcal{P}^N x \in \mathcal{V}^N$, then by $\mathcal{P}^N \to I$ strongly, we have $\|x - x^N\|_{\mathcal{V}} = \|x - \mathcal{P}^N x\|_{\mathcal{V}} \to 0$.

From the definition $\hat{\mathcal{A}} = \mathcal{T}(\tau)$ and $\hat{\mathcal{A}}^N = \mathcal{T}^N(\tau)$, we immediately get that $\hat{\mathcal{A}}^N \mathcal{P}^N \to \hat{\mathcal{A}}$ strongly in $\mathcal{V}$ as $N \to \infty$. Weak convergence of the adjoint of $\hat{\mathcal{A}}^N$, $(\hat{\mathcal{A}}^N)^*$, which is also a bounded operator on $\mathcal{V}^N$, then immediately follows.

Corollary 1. *Let $(\hat{\mathcal{A}}^N)^*$, $\hat{\mathcal{A}}^*$ and $\mathcal{P}^N$ be defined as before. Then $(\hat{\mathcal{A}}^N)^* \mathcal{P}^N \rightharpoonup \hat{\mathcal{A}}^*$ (i.e., weakly) in $\mathcal{V}$.*

Proof. For any φ, ψ in $\mathcal{V}$, we have

$$\begin{aligned}&\langle (\hat{\mathcal{A}}^N)^* \mathcal{P}^N \varphi, \psi \rangle = \langle \mathcal{P}^N (\hat{\mathcal{A}}^N)^* \mathcal{P}^N \varphi, \psi \rangle = \langle (\hat{\mathcal{A}}^N)^* \mathcal{P}^N \varphi, \mathcal{P}^N \psi \rangle \\ &= \langle \mathcal{P}^N \varphi, \hat{\mathcal{A}}^N \mathcal{P}^N \psi \rangle = \langle \varphi, \mathcal{P}^N \hat{\mathcal{A}}^N \mathcal{P}^N \psi \rangle = \langle \varphi, \hat{\mathcal{A}}^N \mathcal{P}^N \psi \rangle,\end{aligned}$$

where the inner product in the above calculation is the $\mathcal{V}$ inner product. Since $\hat{\mathcal{A}}^N \mathcal{P}^N \to \hat{\mathcal{A}}$ strongly in $\mathcal{V}$ as $N \to \infty$, we have $\langle (\hat{\mathcal{A}}^N)^* \mathcal{P}^N \varphi, \psi \rangle \to \langle \varphi, \hat{\mathcal{A}} \psi \rangle = \langle \hat{\mathcal{A}}^* \varphi, \psi \rangle$. ∎

We note that the Trotter–Kato theorem can also be used to argue that $\mathcal{T}^N(t)\mathcal{P}^N x \to \mathcal{T}(t)x$ in the $\mathcal{H}$ norm for $t > 0$, uniformly in t on compact sub intervals. Moreover, since the operator $\mathcal{A}$ is regularly dissipative (see Reference 39), the same arguments can also be used to argue that $(\mathcal{T}^N)^*(t)\mathcal{P}^N x \to \mathcal{T}(t)^* x$ in the $\mathcal{H}$ norm for $t > 0$, uniformly in t on compact sub intervals and consequently that both $\hat{\mathcal{A}}^N$ and $(\hat{\mathcal{A}}^N)^*$ converge to $\hat{\mathcal{A}}$ and $(\hat{\mathcal{A}})^*$, respectively, strongly in $\mathcal{H}$. However, it is worth noting that for some problems of interest the observation operator is bounded in $\mathcal{V}$ but unbounded in $\mathcal{H}$, and

in such a case, one may want to apply the LQR theory to be discussed below in Sections 4.1 and 4.2 in $\mathcal{V}$ rather than in $\mathcal{H}$. In this event, arguing strong convergence of the adjoint may be difficult or simply not true, in which case, weaker convergence results for the approximating solutions to the LQR problem will have to suffice.

4 | AN LQG COMPENSATOR FOR INTRAVENOUS ALCOHOL INFUSION WITH TRANSDERMAL SENSING

We begin by demonstrating how the system (3), (4) in Section 2.2 can be reformulated as an abstract parabolic system in a Gelfand triple of Hilbert spaces as in Section 3.1. Let Q be a compact subset of the positive orthant of $\mathbb{R}^8$, let $H = \mathbb{R}^2 \times L^2(0,1)$ be endowed with the standard inner product and norm and for $q \in Q$, let $H_q = \mathbb{R}^2 \times L^2(0,1)$ with the inner product

$$\langle(\theta,\xi,\varphi),(\overline{\theta},\overline{\xi},\overline{\varphi})\rangle_q = \frac{q_1}{q_3}\theta\overline{\theta} + \frac{q_1}{q_5}\xi\overline{\xi} + \int_0^1 \varphi(\eta)\overline{\varphi}(\eta)d\eta.$$

Let V be the Hilbert space

$$\begin{aligned} V &= \left\{(\theta,\xi,\varphi) \in H : \varphi \in H^1(0,1), \theta = \varphi(0), \xi = \varphi(1)\right\}, \\ &\langle(\varphi(0),\varphi(1),\varphi),(\overline{\varphi}(0),\overline{\varphi}(1),\overline{\varphi})\rangle_V = \varphi(0)\overline{\varphi}(0) + \varphi(1)\overline{\varphi}(1) + \langle\varphi,\overline{\varphi}\rangle_{H^1(0,1)}, \end{aligned}$$

where $\langle\cdot,\cdot\rangle_{H^1(0,1)}$ denotes the standard inner product on $H^1(0,1)$. Standard arguments yield the dense and continuous embeddings $V \hookrightarrow H_q \hookrightarrow V^*$ and that Assumption 4 is satisfied. Define the bilinear form $a(q;\cdot,\cdot)\colon V \times V \to \mathbb{R}$ by

$$a(q;(\varphi(0),\varphi(1),\varphi),(\overline{\varphi}(0),\overline{\varphi}(1),\overline{\varphi})) = \frac{q_1q_4}{q_3}\varphi(0)\overline{\varphi}(0) + \frac{q_1\tilde{q}_6}{q_5}\varphi(1)\overline{\varphi}(1) + q_1\int_0^1 \varphi'(\eta)\overline{\varphi}'(\eta)d\eta, \tag{21}$$

where $\tilde{q}_6 = q_6 + q_L$. Our continuity and compactness assumptions and a simple calculation yield that $a(q;\cdot,\cdot)$ given in (21) satisfies Assumptions 1–3 with all constants appearing in those assumptions independent of $q \in Q$.

For $\hat{\varphi} \in \mathrm{Dom}(A(q))$, define $A(q)\colon \mathrm{Dom}(A(q)) \subset H \to H$ by: $\langle A(q)\hat{\varphi},\hat{\psi}\rangle_{V^*,V} = -a(q;\hat{\varphi},\hat{\psi})$, and $\hat{\psi} \in V$, where $\mathrm{Dom}(A(q)) = \left\{\hat{\varphi} = (\varphi(0),\varphi(1),\varphi) \in V : \varphi \in H^2(0,1)\right\}$ is independent of $q \in Q$. It is not difficult to show that for $\hat{\varphi} = (\varphi(0),\varphi(1),\varphi) \in \mathrm{Dom}(A(q))$, we have $A(q)\hat{\varphi} = A(q)(\varphi(0),\varphi(1),\varphi) = \left(q_3\varphi'(0) - q_4\varphi(0), -q_5\varphi'(1) - \tilde{q}_6\varphi(1), q_1\varphi''\right)$, and that the operator $A(q)$ is densely defined on H_q, regularly dissipative (see, e.g., Reference 39) and self-adjoint. Consequently $A(q)$ is the infinitesimal generator of a uniformly exponentially stable, self-adjoint, analytic semigroup of bounded linear operators, $\{T(q;t) : t \geq 0\}$, on H_q (see, e.g., References 39 and 52).

The variable to be controlled or regulated is v; consequently we define the controlled variable operator $D \in \mathcal{L}(H_q,\mathbb{R})$ by $D(\theta,\xi,\varphi) = \sqrt{\nu}\xi$, $\nu > 0$. The observed state variable is w and therefore the observation or output operator $C \in \mathcal{L}(H_q,\mathbb{R})$ is given by $C(\theta,\xi,\varphi) = \theta$. For $q \in Q$, the input operator $B(q) \in \mathcal{L}(\mathbb{R},H_q)$ is given by $B(q)u = (0,q_2u,0)$, and the random noise influence operator $B_1 \in \mathcal{L}(\mathbb{R}^2,H_q)$ by $B_1\omega = (\omega_1,\omega_2,0)$. In this example, we have $U = Y = Z = \mathbb{R}$, all of which are clearly finite-dimensional. For the finite-time horizon problem, if a terminal penalty is to be included, the operator $G \in \mathcal{L}(H_q,H_q)$ would most likely be chosen to be $G = \rho D^*D$, for some nonnegative weight ρ. We assume zero-order hold input and random noise with sampling interval $\tau > 0$, let $\hat{r} > 0$, and consider the performance index

$$\hat{J}(u) = \mathbb{E}_\pi\left\{\sum_{k=k_0}^{k_1-1}\langle\hat{Q}x_k,x_k\rangle_q + \hat{r}u_k^2 + \langle\hat{G}x_{k_1},x_{k_1}\rangle_q\right\}, \tag{22}$$

where k_1 can be either finite or infinite (in the latter case, $\rho = 0$), and x_k is given by the recurrence $x_{k+1} = \hat{A}(q)x_k + \hat{B}(q)u_k + \hat{B}_1(q)\omega(k\tau)$, $x_0 = (w(0),v(0),x(0,\cdot))$, with $\omega(t) = [\omega_1(t),\omega_2(t)]^T$, $\hat{A}(q) = T(q;\tau) \in \mathcal{L}(H_q,H_q)$ and, recalling that $A(q)$ is coercive, that $\hat{B}(q) = A(q)^{-1}(\hat{A}(q) - I)B(q) \in \mathcal{L}(\mathbb{R},H_q) = H_q$ with $\hat{B}(q) \in \mathrm{Dom}(A(q))$, and

$\hat{B}_1(q) = A(q)^{-1}(\hat{A}(q) - I)B_1 \in \mathcal{L}(\mathbb{R}^2, H_q) = H_q \times H_q$ with $\hat{B}_1(q) \in \text{Dom}(A(q)) \times \text{Dom}(A(q))$. Furthermore, it follows that $\hat{C} = C$ and $\hat{D} = D$, $\hat{Q} = \hat{D}^* \hat{D} \in \mathcal{L}(H_q, H_q)$, $\hat{G} = \rho \hat{D}^* \hat{D} \in \mathcal{L}(H_q, H_q)$, and $\hat{R} = \hat{r}$.

In the observer or estimator, the state covariance operator and output covariance matrix are given by $\tilde{Q}(q) = \hat{B}_1(q)\Sigma\hat{B}_1(q)^* \in \mathcal{L}(H_q, H_q)$ where $\Sigma = \text{diag}(\sigma_1^2, \sigma_2^2) \in \mathbb{R}^{2\times 2}$, and $\tilde{R} = \sigma^2 \in \mathbb{R}$, respectively.

With regard to the semilinear model, we note that our nonlinearity is given by $f(\xi; q) = -\frac{q_7 \xi}{q_8 + \xi}$, $\xi \in \mathbb{R}$, and therefore that $F(\hat{\varphi}; q) = (0, f(\xi; q), 0)$, where $\hat{\varphi} = (\theta, \xi, \phi) \in H$. If we consider the semilinear hybrid PDE/ODE system given in (2), first note that the control input, $\hat{u}$, being the intravenous flow rate of ethanol solution, must always be nonnegative. This of course must be the case even if constraints were not imposed as part of the design process since there is no way that our controller can remove ethanol from the body; we must rely on the liver to do this for us. Since we will rely on a standard LQ design, we will not impose constraints on the controller. However, as will become clear below when we discuss our numerical findings, appropriate choices for the output and control penalty weights in the quadratic performance index and not requiring too steep of a drop in BAC level, yield a control input that is nonnegative. We note further that as with any biomedical feedback controller, for example, an artificial pancreas to control diabetes, any design would include fault detection and patient safety guardrails. Consequently in our case here, the control would have independently applied upper and lower bounds, with the lower bound zero. The fact that the controller is nonnegative, standard maximum principle arguments, and $\hat{x}$, being the solution to a heat equation on the bounded (spatial) domain, $[0, 1]$, yield that $\hat{x}$, and therefore $\hat{w}$ and $\hat{v}$ as well, must all always be nonnegative. On the other hand, the fact that we assumed that the parameter space, Q, is compact in $\mathbb{R}^8$ and therefore closed and bounded. Using a Gronwall inequality argument, it is not difficult to argue that there exists $L > 0$ such that $0 \le \hat{v}(t) \le L$, for all $t \in [0, T]$. Straight forward estimates then yield that f and therefore F and $\mathcal{F}$ as well, are all uniformly Lipschitz continuous as mappings from $[0, T] \times \mathcal{X}$ into $\mathcal{X}$, where $\mathcal{X}$ is $\mathbb{R}$, H, or $\mathcal{H}$, respectively. Turning our attention next to the population models as defined in Section 3.2, let q be a random vector with support Q and distribution described by the probability measure π with all functions involving q π-measurable. Let $\mathcal{V}$ be the Bochner space $\mathcal{V} = L^2_\pi(Q; V)$ and let $\mathcal{V}^*$ be its dual. Let $\mathcal{H} = L^2_\pi(Q; H_q)$, and identify the Hilbert space $\mathcal{H}$ with its dual to obtain the Gelfand triple $\mathcal{V} \hookrightarrow \mathcal{H} \hookrightarrow \mathcal{V}^*$. Define the bilinear form $a(\cdot, \cdot)$ on $\mathcal{V} \times \mathcal{V}$ and the operator $\mathcal{A} \in \mathcal{L}(\mathcal{V}, \mathcal{V}^*)$ by:

$$a(\hat{\varphi}, \hat{\psi}) = \mathbb{E}_\pi\{a(q; \hat{\varphi}(q), \hat{\psi}(q))\} = \int_Q a(q; \hat{\varphi}(q), \hat{\psi}(q)) d\pi(q) = -\langle \mathcal{A}\hat{\varphi}, \hat{\psi} \rangle_{\mathcal{V}^*, \mathcal{V}},$$

for $\hat{\varphi}, \hat{\psi} \in \mathcal{V}$. As in the deterministic setting, the operator $\mathcal{A}$ is regularly dissipative (see, e.g., Reference 39) and self-adjoint and can be restricted to $\text{Dom}(\mathcal{A}) = \{\varphi \in \mathcal{V} : \mathcal{A}\varphi \in \mathcal{H}\}$ as the infinitesimal generator of a uniformly exponentially stable, analytic semigroup $\{\mathcal{T}(t) : t \ge 0\}$ of bounded, self-adjoint, linear operators on $\mathcal{H}$.

Define the operators $\mathcal{B} \in \mathcal{L}(\mathbb{R}, \mathcal{H})$, $\mathcal{B}_1 \in \mathcal{L}(\mathbb{R}^2, \mathcal{H})$, and $\mathcal{C}, \mathcal{D} \in \mathcal{L}(\mathcal{H}, \mathbb{R})$ by $\langle \mathcal{B}u, \mathcal{f} \rangle = \langle B(\cdot)u, \mathcal{f} \rangle_{\mathcal{H}}$, $\mathcal{f} \in \mathcal{H}$, $u \in \mathbb{R}$, $\langle \mathcal{B}_1\omega, \mathcal{f} \rangle = \langle B_1\omega, \mathcal{f} \rangle_{\mathcal{H}}$, $\mathcal{f} \in \mathcal{H}$, $\omega \in \mathbb{R}^2$, $\mathcal{C}\hat{\varphi} = \mathbb{E}_\pi\{C\hat{\varphi}\}$, and $\mathcal{D}\hat{\varphi} = \mathbb{E}_\pi\{D\hat{\varphi}\}$, $\hat{\varphi} \in \mathcal{H}$, respectively. Then set $\hat{\mathcal{A}} = \mathcal{T}(\tau) \in \mathcal{L}(\mathcal{H}, \mathcal{H})$, $\hat{\mathcal{B}} = \mathcal{A}^{-1}(\hat{\mathcal{A}} - \mathcal{I})\mathcal{B} \in \mathcal{L}(\mathbb{R}, \mathcal{H})$, $\hat{\mathcal{B}}_1 = \mathcal{A}^{-1}(\hat{\mathcal{A}} - \mathcal{I})\mathcal{B}_1 \in \mathcal{L}(\mathbb{R}^2, \mathcal{H})$, $\hat{\mathcal{C}} = \mathcal{C} \in \mathcal{L}(\mathcal{H}, \mathbb{R})$, and $\hat{\mathcal{D}} = \mathcal{D} \in \mathcal{L}(\mathcal{H}, \mathbb{R})$, where $\mathcal{I}$ is the identity on $\mathcal{H}$.

4.1 | The compensator

With these definitions, we then consider the discrete-time linear quadratic regulator problem in $\mathcal{H}$ for the quadratic performance index

$$\hat{\mathcal{J}}(u) = \sum_{k=k_0}^{k_1-1} \langle \hat{\mathcal{Q}} x_k, x_k \rangle_{\mathcal{H}} + \hat{r} u_k^2 + \langle \hat{\mathcal{G}} x_{k_1}, x_{k_1} \rangle_{\mathcal{H}}, \tag{23}$$

subject to the discrete-time linear system

$$\begin{aligned} x_{k+1} &= \hat{\mathcal{A}} x_k + \hat{\mathcal{B}} u_k + \hat{\mathcal{B}}_1 \omega(k\tau), \quad x_0 = \hat{\varphi}_0, \\ y_k &= \hat{\mathcal{C}} x_k + \zeta(k\tau), \quad \varkappa_k = \hat{\mathcal{D}} x_k, \quad k = k_0, k_0 + 1, k_0 + 2, \ldots, \end{aligned} \tag{24}$$

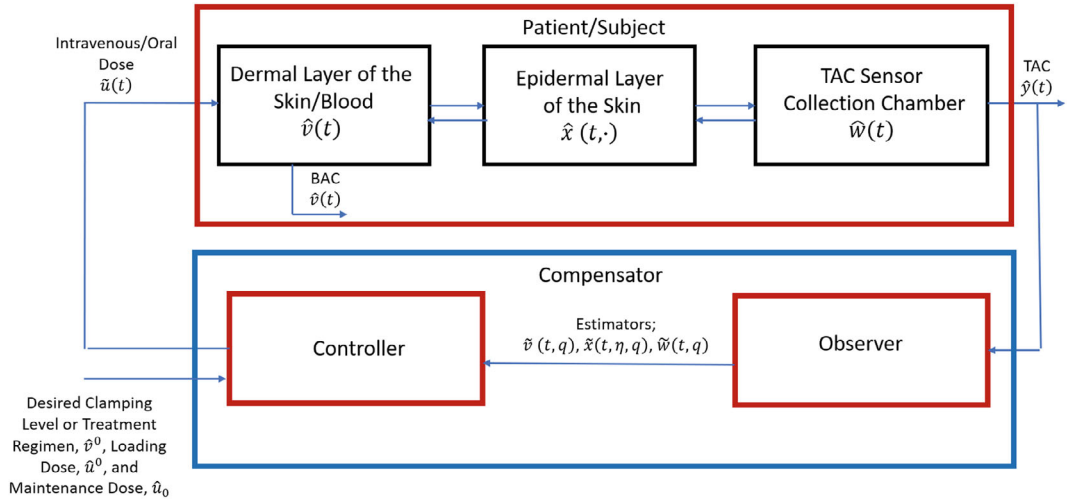

FIGURE 3 Signal flow diagram of the closed-loop system

where $\hat{Q}, \hat{\mathcal{G}} \in \mathcal{L}(\mathcal{H}, \mathcal{H})$ are given by $\hat{Q} = \hat{D}^* \hat{D}$, and $\hat{\mathcal{G}} = \rho \hat{D}^* \hat{D}$, respectively and $\hat{\varphi}_0 \in \mathcal{H}$. Note that in light of our definitions, the quadratic performance index given in (23) is the same as the one given in (22).

In what follows we will only concern ourselves with the infinite horizon problem (i.e., when $k_1 = \infty$ and $\rho = 0$); the results for the finite horizon problem are analogous. By Theorem 5.2 in Reference 53, the uniform exponential stability of the semigroup $\{\mathcal{T}(t) : t \geq 0\}$ and therefore of $\hat{\mathcal{A}}$ as well guarantee that there exists a unique solution to (24), and consequently that an admissible control exists for any initial value. Moreover, by Remark 5.2 in Reference 53, we have for any admissible control, $\lim_{k\to\infty} \|x_k\|_{\mathcal{H}} = 0$. Hence there exists a unique positive semi-definite self-adjoint solution to the algebraic Riccati equation (ARE)

$$\hat{\Pi} = \hat{\mathcal{A}}^* \left[\hat{\Pi} - \hat{\Pi}\hat{\mathcal{B}} \left(\hat{r} + \hat{\mathcal{B}}^* \hat{\Pi} \hat{\mathcal{B}} \right)^{-1} \hat{\mathcal{B}}^* \hat{\Pi} \right] \hat{\mathcal{A}} + \hat{\mathcal{Q}}, \tag{25}$$

the optimal input in closed-loop linear state feedback form is given by:

$$\overline{u}_k = -\hat{\mathcal{F}} \overline{x}_k = -\langle \hat{\ell}, \overline{x}_k \rangle_{\mathcal{H}}, \quad k = k_0, \ k_0 + 1, \ \dots, \tag{26}$$

where

$$\hat{\mathcal{F}} = \left\{ \hat{r} + \hat{\mathcal{B}}^* \hat{\Pi} \hat{\mathcal{B}} \right\}^{-1} \hat{\mathcal{B}}^* \hat{\Pi} \hat{\mathcal{A}}, \tag{27}$$

$\hat{\Pi}$ is given by (25), $\hat{\ell} = \hat{\mathcal{F}}^*$ is the corresponding functional gain, $\hat{\mathcal{J}}(\overline{u}) = \langle \hat{\Pi}\hat{\varphi}_0, \hat{\varphi}_0 \rangle_{\mathcal{H}}$, and that the optimal trajectory $\{\overline{x}_k\}_{k=k_0}^{\infty}$ is given by $\overline{x}_{k+1} = (\hat{\mathcal{A}} - \hat{\mathcal{B}}\hat{\mathcal{F}})\overline{x}_k$, $\overline{x}_0 = \hat{\varphi}_0$ (Figure 3).

To construct the compensator, we couple the feedback control law given by (26) and (27) with a Kalman filter based observer. As in the case of the controller, the fact that the open loop semigroup is self adjoint and uniformly exponentially stable, the Kalman observer tends to steady state as the time horizon tends to infinity.[54] Again, we only treat the steady state case here; in discrete or sampled time, the Hilbert space operator-based theory for the finite time horizon Kalman state estimator is completely analogous to the finite dimensional theory involving matrices. The observer takes the form

$$\tilde{x}_{k+1} = \hat{\mathcal{A}}\tilde{x}_k + \hat{\mathcal{B}}u_k + \tilde{\mathcal{L}}(y(k\tau) - \hat{\mathcal{C}}\tilde{x}_k), \quad \tilde{x}_{k_0} = \tilde{\varphi}_0, \tag{28}$$

$k \geq k_0$, where $\tilde{\varphi}_0 \in \mathcal{H}$ is arbitrary and the operator observer gain $\tilde{\mathcal{L}} \in \mathcal{L}(\mathbb{R}, \mathcal{H})$ in (28) is given by $\tilde{\mathcal{L}} = \hat{\mathcal{A}}\tilde{\Pi}\hat{\mathcal{C}}^* \left\{ \sigma^2 + \hat{\mathcal{C}}\tilde{\Pi}\hat{\mathcal{C}}^* \right\}^{-1}$, with the operator $\tilde{\Pi}$ the unique positive semi-definite self-adjoint solution guaranteed to exist to the ARE given by:

$$\tilde{\Pi} = \hat{\mathcal{A}}\left[\tilde{\Pi} - \tilde{\Pi}\hat{C}^*\left(\sigma^2 + \hat{C}\tilde{\Pi}\hat{C}^*\right)^{-1}\hat{C}\tilde{\Pi}\right]\hat{\mathcal{A}}^* + \tilde{\mathcal{Q}}, \tag{29}$$

where in (29), $\tilde{\mathcal{Q}} = \hat{\mathcal{B}}_1\Sigma\hat{\mathcal{B}}_1^* \in \mathcal{L}(\mathcal{H},\mathcal{H})$.

Combining the controller given in Equations (25) -(27) with the observer given by Equations (28) and (29), the optimal LQG compensator is then given by $\tilde{u}_k = -\hat{\mathcal{F}}\tilde{x}_k = -\langle\hat{\ell}, \tilde{x}_k\rangle_{\mathcal{H}}, k = k_0, k_0+1, k_0+2, \dots$, where the functional control gains $\hat{\ell}$ and the feedback operator $\hat{\mathcal{F}}$ are given by (26) and (27), respectively. Note that since $\tilde{\mathcal{L}} \in \mathcal{L}(\mathbb{R},\mathcal{H})$, it follows that in fact $\tilde{\mathcal{L}} = \tilde{\ell} \in \mathcal{H}$. The element $\tilde{\ell}$ in $\mathcal{H}$ is the optimal functional observer gain. Finally we note that the spectrum for the closed-loop compensator system (23)–(29) is given by:

$$\sigma(\mathcal{S}^{\infty,\infty}) = \sigma\left(\begin{bmatrix}\hat{\mathcal{A}} & -\hat{\mathcal{B}}\hat{\mathcal{F}} \\ \tilde{\mathcal{L}}\hat{C} & \hat{\mathcal{A}} - \hat{\mathcal{B}}\hat{\mathcal{F}} - \tilde{\mathcal{L}}\hat{C}\end{bmatrix}\right), \tag{30}$$

from which it is not difficult to argue that in fact $\sigma(\mathcal{S}) = \sigma(\hat{\mathcal{A}} - \hat{\mathcal{B}}\hat{\mathcal{F}}) \cup \sigma(\hat{\mathcal{A}} - \tilde{\mathcal{L}}\hat{C})$.

When the state equation is taken to be the semilinear model and, as it is in the problem of interest to us here, the nonlinearity in (7) is of the form $F(t,x) = Bf(x)$, for some function $f : H \to \mathbb{R}$, then it is possible to define a nonlinear compensator in which the controller effectively annihilates the nonlinearity and the observer estimates the nonlinear state. Indeed, when the nonlinear system is reformulated in state space form, if both the control input and the nonlinearity are acted upon by essentially the same (more precisely, up to a scalar constant multiple) actuator influence operator (i.e., the $\hat{\mathcal{B}}$ operator), it is possible to design a feedback controller that (1) subtracts the nonlinearity from the plant, (2) linearly feeds back the difference between the state of the nonlinear plant and the equilibrium state of the nonlinear plant, (3) adds the nonlinearity evaluated at the equilibrium state, and (4) adds the equilibrium input. It is then not difficult to show that if the linear feedback law is designed to regulate the linear part of the nonlinear plant, the closed loop nonlinear plant will return to, and operate at, the equilibrium state, as desired. In this case, the controller given in (26) now takes the form

$$\tilde{u}_k = -\hat{\mathcal{F}}_k(\tilde{x}_k - x_0) - f(\tilde{x}_k) + f(x_0) + \hat{u}_0, \tag{31}$$

where x_0 is the target steady state or equilibrium solution, x_0 is the constant function $x_0 \in \mathcal{H}$ given by $x_0(q) = x_0$, for $q \in Q$, and $\hat{u}_0$ is the maintenance or steady state input. This controller given in (31) will necessarily require an observer that estimates the nonlinear state. One such nonlinear observer is given below in (32) as

$$\tilde{x}_{k+1} = \hat{\mathcal{A}}\tilde{x}_k + \hat{\mathcal{B}}\tilde{u}_k + \hat{\mathcal{B}}f(\tilde{x}_k) + \tilde{\mathcal{L}}(\tilde{y}(k\tau) - \hat{C}\tilde{x}_k). \tag{32}$$

4.2 | Finite-dimensional approximation and convergence

The approximation and convergence theory presented in References 34, 37, 40, and 42 tells us how to proceed here. We need only describe (1) how to construct a sequence of finite-dimensional approximating subspaces of $\mathcal{V}$, $\mathcal{V}^N$, whose corresponding sequence of orthogonal projections converges strongly to the identity in $\mathcal{V}$, and (2) how to define appropriately converging sequences of approximating operators to $\hat{\mathcal{B}}$, $\hat{C}$, $\hat{\mathcal{D}}$, and $\tilde{\mathcal{Q}}$.

Let N represent the multi-index $N = (n, m_1, m_2, \dots, m_8)$ and when we write $N \to \infty$, we mean $n \to \infty$ and $m_i \to \infty$, $i = 1, 2, \dots, 8$. We assume that the random parameter q_i has support $[a_i, b_i]$, $i = 1, 2, \dots, 8$, all assumed to be bounded. Let Q be the compact subset of $\mathbb{R}^8$ given by $Q = \times_{i=1}^{8}[a_i, b_i]$. For $i = 1, 2, \dots, 8$, partition $[a_i, b_i]$ into m_i equal subintervals, and let $\chi_j^{m_i}$ denote the characteristic function of the jth subinterval, $j = 1, 2, \dots, m_i$. For $n = 1, 2, \dots$ let $\{\varphi_j^n\}_{j=0}^n$ denote the standard linear B-splines on $[0,1]$ with respect to the uniform mesh $\{0, \frac{1}{n}, \frac{2}{n}, \dots, 1\}$ and set $\hat{\varphi}_j^n = (\varphi_j^n(0), \varphi_j^n(1), \varphi_j^n) \in V$. Let J denote a multi-index of the form $J = (j_0, j_1, \dots, j_8)$ where $j_0 \in \{0, 1, 2, \dots, n\}$ and $j_i \in \{1, 2, \dots, m_i\}$, $i = 1, 2, \dots, 8$. Then set $\Phi_J^N = \hat{\varphi}_{j_0}^n \Pi_{i=1}^8 \chi_{j_i}^{m_i}$, let $\mathcal{V}^N = \text{span}_J\{\Phi_J^N\}$, and let $\mathcal{P}^N : \mathcal{H} \to \mathcal{V}^N$ denote the orthogonal projection of $\mathcal{H}$ onto $\mathcal{V}^N$. Standard arguments from the theory of splines and piecewise constant approximation in L^2 can be used to argue that $\mathcal{P}^N$ converges strongly to the identity in both $\mathcal{H}$ and $\mathcal{V}$.

Since $\mathcal{V}^N$ is a subspace of $\mathcal{V}$ (and therefore $\mathcal{H}$ as well) we simply set $\hat{C}^N = \hat{C}\mathcal{P}^N$ for all multi-indices N. We obtain $\mathcal{A}^N \in \mathcal{L}(\mathcal{V}^N, \mathcal{V}^N)$ via a Galerkin approach as described in Section 3.3 and set $\hat{\mathcal{A}}^N = \exp(\mathcal{A}^N\tau) \in \mathcal{L}(\mathcal{V}^N, \mathcal{V}^N)$. We then set $\hat{\mathcal{B}}^N = (\mathcal{A}^N)^{-1}(\hat{\mathcal{A}}^N - \mathcal{I}^N)\mathcal{P}^N\mathcal{B} \in \mathcal{L}(\mathbb{R}, \mathcal{V}^N)$. Similarly we set $\hat{\mathcal{B}}_1^N = (\mathcal{A}^N)^{-1}(\hat{\mathcal{A}}^N - \mathcal{I}^N)\mathcal{P}^N\mathcal{B}_1 \in \mathcal{L}(\mathbb{R}^2, \mathcal{V}^N)$, and then set $\tilde{\mathcal{Q}}^N = \hat{\mathcal{B}}_1^N\Sigma(\hat{\mathcal{B}}_1^N)^* \in \mathcal{L}(\mathcal{V}^N, \mathcal{V}^N)$. We note also that $\hat{\mathcal{Q}}^N = \mathcal{P}^N\hat{\mathcal{Q}}\mathcal{P}^N = (\hat{\mathcal{D}}^N)^*\hat{\mathcal{D}}^N$, where $\hat{\mathcal{D}}^N = \hat{\mathcal{D}}\mathcal{P}^N$. Standard arguments from functional analysis (specifically, linear semigroup theory) (see, e.g., References 34 and 42) can then be used to argue the requisite convergence.

We consider the finite-dimensional approximating infinite-time horizon LQG compensator problems of minimizing

$$\hat{\mathcal{J}}^N(u^N) = \sum_{k=k_0}^{\infty} \langle \hat{\mathcal{Q}}^N x_k^N, x_k^N\rangle_{\mathcal{H}} + \hat{r}(u_k^N)^2$$

subject to

$$\begin{aligned} x_{k+1}^N &= \hat{\mathcal{A}}^N x_k^N + \hat{\mathcal{B}}^N u_k^N + \hat{\mathcal{B}}_1^N \omega(k\tau),\ x_0^N = \mathcal{P}^N\hat{\varphi}_0, \\ y_k^N &= \hat{C}^N x_k^N + \zeta(k\tau), \quad z_k^N = \hat{\mathcal{D}}^N x_k^N, \quad k = k_0, k_0+1, \dots . \end{aligned} \tag{33}$$

As in the infinite-dimensional case, the unique solution to this control problem is given in closed-loop linear state feedback form by (see References 42 and 54)

$$\overline{u}_k^N = -\hat{\mathcal{F}}^N\overline{x}_k^N = -\langle \hat{\mathcal{F}}^N, \overline{x}_k^N\rangle_{\mathcal{H}}, \quad k = k_0,\ k_0+1, \dots , \tag{34}$$

where

$$\hat{\mathcal{F}}^N = \left\{\hat{r} + (\hat{\mathcal{B}}^N)^*\hat{\Pi}^N\hat{\mathcal{B}}^N\right\}^{-1}(\hat{\mathcal{B}}^N)^*\hat{\Pi}^N\hat{\mathcal{A}}^N, \tag{35}$$

and $\hat{\Pi}^N$ is the unique positive semi-definite, symmetric solution to the approximating ARE,

$$\hat{\Pi}^N = (\hat{\mathcal{A}}^N)^*\left[\hat{\Pi}^N - \hat{\Pi}^N\hat{\mathcal{B}}^N\left(\hat{r} + (\hat{\mathcal{B}}^N)^*\hat{\Pi}^N\hat{\mathcal{B}}^N\right)^{-1}(\hat{\mathcal{B}}^N)^*\hat{\Pi}^N\right]\hat{\mathcal{A}}^N + (\hat{\mathcal{D}}^N)^*\hat{\mathcal{D}}^N, \tag{36}$$

where $\overline{x}_k^N$ denotes the trajectory given by (33) with $u_k^N = \overline{u}_k^N$, $k = k_0, k_0+1, \dots$ and $\hat{\mathcal{F}}^N$ denotes the optimal functional control gains. It follows that $\hat{\mathcal{J}}^N(\overline{u}^N) = \langle\hat{\Pi}^N\mathcal{P}^N\hat{\varphi}_0, \mathcal{P}^N\hat{\varphi}_0\rangle_{\mathcal{H}}$ and that the optimal trajectory is given by $\overline{x}_{k+1}^N = \left(\hat{\mathcal{A}}^N - \hat{\mathcal{B}}^N\hat{\mathcal{F}}^N\right)\overline{x}_k^N$, $x_0^N = \mathcal{P}^N\hat{\varphi}_0$. We note that in actual practice, the control applied would be $\overline{u}_k^N = -\langle\hat{\mathcal{F}}^N, \overline{x}_k\rangle_{\mathcal{H}}$, $k = k_0,\ k_0+1, \dots$, where $\overline{x}_k$ denotes the trajectory given by (24) with $u_k = \overline{u}_k^N$, $k = k_0, k_0+1, \dots$.

The approximating observer is given by:

$$\tilde{x}_{k+1}^N = \hat{\mathcal{A}}^N\tilde{x}_k^N + \hat{\mathcal{B}}^N u_k^N + \tilde{\mathcal{L}}^N(y(k\tau) - \hat{C}^N\tilde{x}_k^N), \tag{37}$$

with $\tilde{x}_0^N = \mathcal{P}^N\tilde{\varphi}_0$, where $\tilde{\mathcal{L}}^N \in \mathcal{L}(\mathbb{R}, \mathcal{V}^N)$ is given by:

$$\tilde{\mathcal{L}}^N = \hat{\mathcal{A}}^N\tilde{\Pi}^N\hat{C}^*\left\{\sigma^2 + \hat{C}^N\tilde{\Pi}^N(\hat{C}^N)^*\right\}^{-1}, \tag{38}$$

with $\tilde{\Pi}^N$ the unique positive semi-definite symmetric solution to the ARE

$$\tilde{\Pi}^N = \hat{\mathcal{A}}^N\left[\tilde{\Pi}^N - \tilde{\Pi}^N(\hat{C}^N)^*\left(\sigma^2 + \hat{C}^N\tilde{\Pi}^N(\hat{C}^N)^*\right)^{-1}\hat{C}^N\tilde{\Pi}^N\right](\hat{\mathcal{A}}^N)^* + \hat{\mathcal{B}}_1^N\Sigma(\hat{\mathcal{B}}_1^N)^*. \tag{39}$$

Equations (33)–(39) are all operator equations, albeit finite-dimensional ones. In order to actually carry out computations (i.e., by using standard ARE solvers, see Reference 54) these equations must be converted to equivalent matrix

equations. Since the basis we have chosen for $\mathcal{V}^N$ is not orthonormal, some care must be exercised in making this conversion so as to obtain a standard symmetric matrix ARE. The details are found in References 34 or 42.

Combining the approximating finite dimensional controller given by (34)–(36) with the approximating finite dimensional observer given by (37)–(39), the approximating finite dimensional compensator is then given by:

$$\begin{aligned}\overline{u}_k^N &= -\hat{F}^N \tilde{x}_k^N = -\langle \hat{\ell}^N, \tilde{x}_k^N \rangle_{\mathcal{H}} \\ &= -\int_Q \left\{ \frac{q_1}{q_3} \hat{\ell}_3^N(0,q)\tilde{x}_{3,k}^N(0,q) + \frac{q_1}{q_5}\hat{\ell}_3^N(1,q)\tilde{x}_{3,k}^N(1,q) + \int_0^1 \hat{\ell}_3^N(\eta,q)\tilde{x}_{3,k}^N(\eta,q)d\eta \right\} d\pi(q), \quad k = k_0,\ k_0+1,\ \dots, \end{aligned} \tag{40}$$

where in the above expression (40) we have used the following notational convention $\hat{\ell}^N = (\hat{\ell}_1^N, \hat{\ell}_2^N, \hat{\ell}_3^N) \in \mathcal{V}^N$ and $\tilde{x}_k^N = (\tilde{x}_{1,k}^N, \tilde{x}_{2,k}^N, \tilde{x}_{3,k}^N) \in \mathcal{V}^N$ given by (37). We note that because the generator $\mathcal{A}^N$ of the approximating semigroup $\{\exp(\mathcal{A}^N t) : t \geq 0\}$, was constructed using a Galerkin approach, we are guaranteed the existence of unique positive semi-definite symmetric solutions to the AREs for the same reasons that this is true in the infinite-dimensional case stated in the previous sub-section (see References 34 and 42). In addition, the convergence results given in References 34 and 42 apply. Finally we note that analogously to (30), the closed-loop system with the approximating observer and feedback control law is given by

$$\sigma(\mathcal{S}^{\infty,N}) = \sigma\left(\begin{bmatrix} \hat{\mathcal{A}} & -\hat{\mathcal{B}}\hat{\mathcal{F}}^N \\ \tilde{\mathcal{L}}^N\hat{\mathcal{C}} & \hat{\mathcal{A}}^N - \hat{\mathcal{B}}^N\hat{\mathcal{F}}^N - \tilde{\mathcal{L}}^N\hat{\mathcal{C}}^N \end{bmatrix}\right),$$

with the approximating closed loop eigenvalues given by

$$\begin{aligned}\sigma(\mathcal{S}^{N,N}) &= \sigma\left(\begin{bmatrix} \hat{\mathcal{A}}^N & -\hat{\mathcal{B}}^N\hat{\mathcal{F}}^N \\ \tilde{\mathcal{L}}^N\hat{\mathcal{C}}^N & \hat{\mathcal{A}}^N - \hat{\mathcal{B}}^N\hat{F}^N - \tilde{\mathcal{L}}^N\hat{\mathcal{C}}^N \end{bmatrix}\right) \\ &= \sigma(\hat{\mathcal{A}}^N - \hat{\mathcal{B}}^N\hat{\mathcal{F}}^N) \cup \sigma(\hat{\mathcal{A}}^N - \tilde{\mathcal{L}}^N\hat{\mathcal{C}}^N).\end{aligned}$$

We note that approximation and convergence for the nonlinear compensator given by (31) and (32) are analogous to the results presented here for the linear compensator.

5 | FITTING AND VALIDATION OF THE INDIVIDUAL AND POPULATION MODELS AND THE STATE ESTIMATOR

Since values for most of the parameters that appear in the model (1) cannot be found in the literature, and the few that can are typically based on in-vitro rather than in-vivo studies, validation via forward simulation is not a possibility. Rather, we validate the model (2) by using inverse problem techniques to demonstrate that it can be fit to human subject data collected in the Luczak Laboratory in the Department of Psychology at the University of Southern California with IRB approval. Since a substantial amount of data for intravenously infused alcohol does not exist, the BrAC/TAC data we used were from studies involving oral dosing administered in the form of a bolus of ethanol mixed with fruit juice. We note that the model given in (2) continues to hold in this case, albeit with minor adjustment to the interpretation of the actuator gain, q_2. Our studies indicated that while the model can be fit to data collected at different times from a large and diverse cohort of subjects wearing different TAC sensors, the resulting values of the parameters vary across the population.

5.1 | Human subject validation data

To validate the models, we used BrAC, TAC, and covariate data collected in a controlled laboratory environment from 40 participants (50% female, ages 21–33 years, 35% BMI >25.0). Each participant orally consumed the same alcohol dose

in four drinking sessions on four different days. Dosing for these sessions was determined by the regression-determined Widmark equations for males and females, which calculate an estimated total body water (TBW) for each person to determine how much alcohol is needed to bring him/her to a specified blood alcohol level.[49,55,56] The formulas are $TBW = -2.097 + (0.1069 \times HEIGHT) + (0.2466 \times WEIGHT)$ for females and $TBW = 2.447 - (0.09516 \times AGE) + (0.1074 \times HEIGHT) + (0.3362 \times WEIGHT)$ for males, where height is in centimeters and weight is in kilograms. Then the alcohol Dose for both males and females was given in milliliters by Alcohol dose $= 1.2 \times TBW/0.4$. The alcohol used was vodka with an ethanol content of 40%, which was mixed with fruit juice and sugar-free carbonated soda so participants were not drinking pure alcohol.

For each drinking session, the alcohol dose was consumed in one of three predetermined patterns, in which the dose was (1) consumed evenly across a 15-min period, (2) divided into two portions, which were consumed in two 15-min periods with a 30 min break in between, or (3) divided into six portions, which were consumed every 10 min over an hour. During each session, participant BrAC was measured via breath analyzer (Intoximeters, Inc., St. Louis, MO), and two sets of TAC were measured at the upper arm via SCRAM-CAM TAC sensors (Alcohol Monitoring Systems, AMS, Littleton, CO). BrAC and TAC were obtained at 10-min intervals while participants' BrAC remained above 0.000, after which the TAC devices continued to obtain readings at 30-min intervals until TAC also reached 0.000. After excluding some datasets due to a change in our data collection protocol, and because some participants did not complete all four sessions, our final analytic sample consists of 267 BrAC/TAC datasets, 140 from males and 127 from females.

Although we did not make use of this in the present study, the data also included covariates that may affect the BrAC/TAC relationship, and could therefore be used to improve accuracy by either incorporating them into the model or using them to further stratify the data so as to reduce the variance in the distributions of the fit parameters. The collected covariates included sex, age, race/ethnicity, body measurement data (e.g., BMI, waist to hip ratio, percent body fat), and data on subject drinking behavior 28 and 90 days prior to study participation (which could affect alcohol metabolism). Session-level covariates included alcohol administration pattern and blood pressure readings (at baseline, session high, and session low). The covariates could also be used to fit a regression model that can be used to determine the loading and maintenance doses, $\hat{u}^0$ and $\hat{u}_0$, respectively.

5.2 | Fitting and validation of the individual models

We used the techniques for solving inverse problems for distributed parameter systems developed in, for example, References 11-13, 29, and 52, to estimate the values for the parameters q_i, $i = 1, 2, \ldots, 8$ appearing in (2). The identification or estimation problem for each individual drinking episode is formulated as a nonlinear (in the parameters) least squares fit to data in the form of spline fits to contemporaneously collected sampled-time breathalyzer measurements of BrAC and sampled-time biosensor measurements of TAC. The resulting optimization problems are solved via gradient search techniques with partial derivatives with respect to the parameters being computed using the adjoint method.[57] We did this for the cohort of male participants, female participants, and both groups combined. We report our results for the combined cohort of 267 subjects in Figure 4 and Table 1.

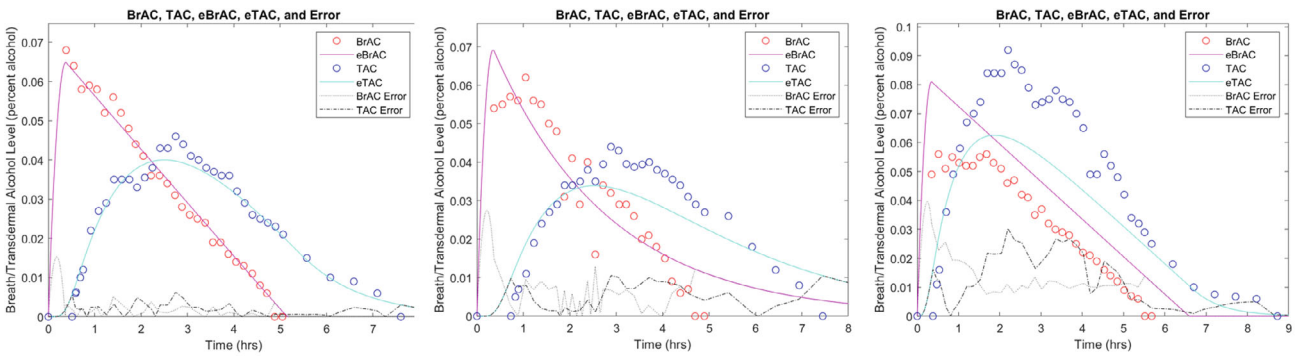

FIGURE 4 Individual subject model validation: Left panel: Fit with small combined BrAC and TAC relative L_1 error (BrAC: 0.05, TAC: 0.08); Center panel: Fit with median combined BrAC and TAC relative L_1 error (BrAC: 0.21, TAC: 0.21); Right panel: Fit with large combined BrAC and TAC relative L_1 error (BrAC: 0.21, TAC: 0.38)

TABLE 1 Validation results for the individual subject model

1	2	3	4	5	6	7	8
0.21	0.21	0.11	0.26	0.68	0.33	0.04	0.07
0.12	0.19	0.10	0.13	0.39	0.35	0.13	0.11

In the three panels of Figure 4, we have plotted the results of fitting the individual model for three of the episodes in the combined cohort. For each episode in the cohort we first used the collected BrAC and TAC data to estimate the model parameters as described above. We then used the fit model, the TAC data, and a non-negatively constrained, H_1 norm regularized, quadratic programming-based linear least squares minimization scheme (the Matlab routine lsqnonneg) to deconvolve an estimate of the BrAC, or eBrAC, based on the fit model. Finally, we input the resampled linear spline interpolation of the BrAC data into the fit model to obtain estimated TAC or eTAC. In each panel we plot the BrAC and TAC data, the eBrAC and eTAC curves and the differences between the data and the estimates. The left panel shows an episode for which the fit was especially good (small combined BrAC and TAC relative L_1 error), the center panel is an episode in which the combined BrAC and TAC relative error was essentially at the median over the entire cohort, and the right panel is a drinking episode for which the combined BrAC and TAC relative error was among the largest in the cohort.

In Table 1, the labeled columns are (1) BrAC relative L_1 error, (2) TAC relative L_1 error, (3) peak BrAC relative error, (4) peak TAC relative error, (5) time of peak BrAC error (h), (6) time of peak TAC error (h), (7) area under BrAC curve relative error, and (8) area under TAC curve relative error. The first row is the median value over the entire male and female combined cohort ($n = 267$) and the second row is the standard deviation. The results for the other two cohorts were similar.

We note that in general, the BrAC/TAC datasets that yielded larger BrAC and TAC relative L_1 errors were in some way anomalous. For example, some had spurious unexplained spikes or dips in either the BrAC or TAC signal. Possible explanations could be the presence of mouth alcohol when the breath reading was taken, incomplete emptying of the transdermal alcohol collection chamber in the TAC sensor, or an insufficient time interval between measurements. In the right panel in Figure 4, the atypical anomaly is the fact that in this episode the measured TAC signal has a higher peak than the BrAC signal. These signal anomalies illustrate the challenge in designing a controller for a highly subject-dependent, physiological bio-chemical process using an electro-chemical sensor that is not entirely isolated from environmental contamination.

5.3 | Fitting and validation of the population model

Once again, using the full cohort of BrAC/TAC data from the 267 subjects, we first eliminated outliers from the fit parameter vectors, $q = [q_1, q_2, \dots, q_8]$ by removing those episodes for which any of the fit parameters were beyond one and one half times the right hand boundary of the third quartile for that parameter. The remaining training set consisted of 95 drinking episodes. To reduce the dimension of the compensator, since the parameters q_i, $i = 4, 5, 6, 7, 8$ were relatively small with small variance, we simply used their sample means, $\overline{q}_4 = 3.9 \times 10^{-1}$, $\overline{q}_5 = 1.6 \times 10^{-4}$, $\overline{q}_6 = 3.6 \times 10^{-4}$, $\overline{q}_7 = 1.1 \times 10^{-2}$, and $\overline{q}_8 = 2.1 \times 10^{-5}$ in the population model.

We used the method of moments (see Reference 58) to fit a scaled beta distribution to q_1, and scaled gamma distributions to q_2 and q_3. We have also used maximum likelihood estimators for the parameters and nonparametric techniques to directly fit a probability density function to the q data, and obtained similar results. The method of moments is a parametric statistical technique in which the p parameters of the estimated distribution are chosen so that the first p theoretical moments match the first p sample moments. Although our theory does not require it, for simplicity, we assumed that q_i, $i = 1, 2, 3$ were independent. The scaling was based on the nth order statistic,[58] $q_{i,(n)}$, $i = 1, 2, 3$. The resulting fits were: $q_1 \sim q_{1,(n)} q_1$ with $q_{1,(n)} = 0.74$ and $q_1 \sim \text{Beta}(3.49, 3.60)$, $q_2 \sim q_{2,(n)} q_2$ with $q_{2,(n)} = 0.71$ and $q_2 \sim \text{Gamma}(8.79, 0.06)$, and $q_3 \sim q_{3,(n)} q_3$ with $q_{3,(n)} = 19.70$ and $q_3 \sim \text{Gamma}(2.08, 0.16)$. In Figure 5, we have plotted the resulting probability density functions of the estimated distributions along with scaled (so that the area is one) histograms of the samples of q_1, q_2, and q_3.

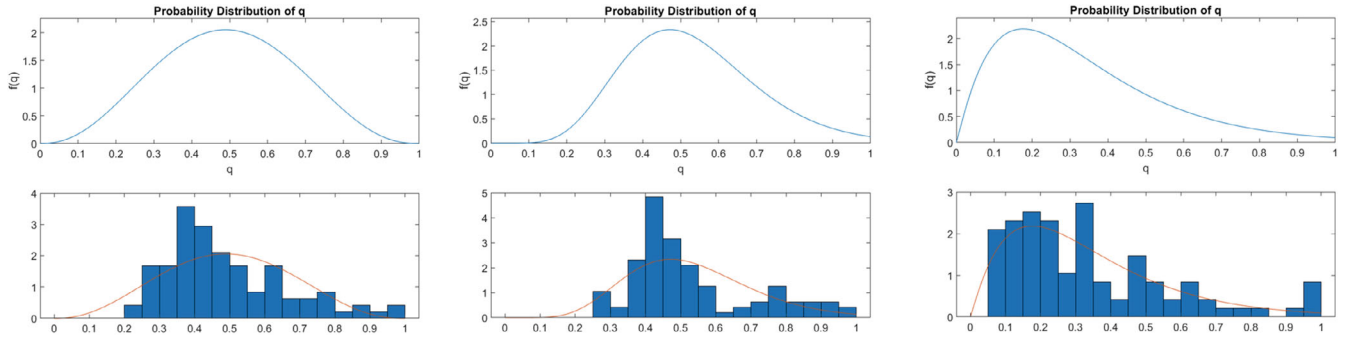

FIGURE 5 Scaled histograms and fit distributions of q_i for the samples of q_i, $i = 1, 2, 3$: Left panel: $q_1 \sim$ Beta(3.49, 3.60); Center panel: $q_2 \sim$ Gamma(8.79, 0.06); Right panel: $q_3 \sim$ Gamma(2.08, 0.16)

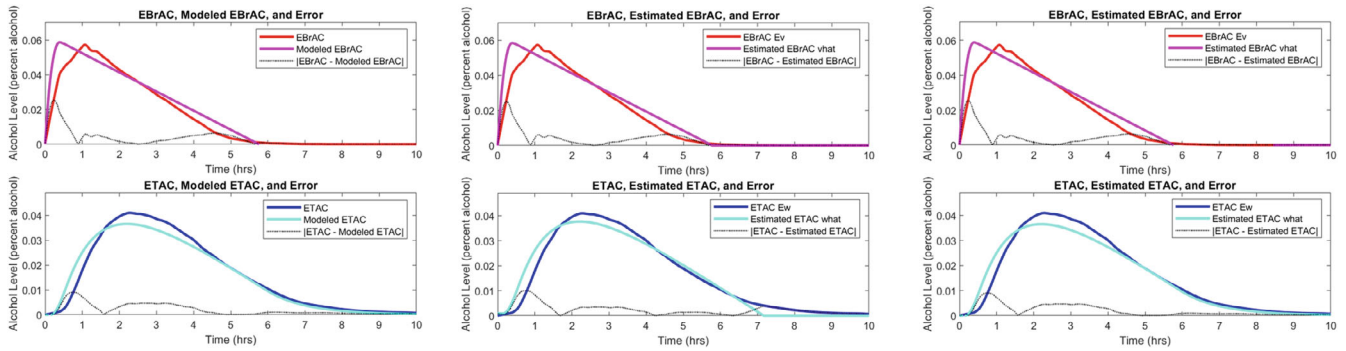

FIGURE 6 Population model validation: Left upper panel: Population mean of the BrAC signal and BrAC signal produced by the population model; Left lower panel: population mean of the TAC signal and TAC signal produced by the population model; linear population state estimator validation: Center upper panel: population mean of the BrAC signal and BrAC signal produced by the linear population estimator; Center lower panel: population mean of the TAC signal and TAC signal produced by the linear population estimator; nonlinear population state estimator validation: Right upper panel: population mean of the BrAC signal and BrAC signal produced by the nonlinear population estimator; Right lower panel: population mean of the TAC signal and TAC signal produced by the nonlinear population estimator

The law of large numbers[58] lets us estimate the expected value of the TAC and BrAC signals for the population by averaging the TAC and BrAC signals across the 267 samples in our dataset. In effect, in doing this we obtain an approximation to the population mean TAC and BrAC response to the oral dosing described in Section 5.1. In addition, once the distributions of the parameters have been fit, and if the oral dosing described in Section 5.1 is modeled as $\{u_k\}$, the quantities $\{y_k\}$ and $\{z_k\}$ in the population model (24) and their finite dimensional approximations $\{y_k^N\}$ and $\{z_k^N\}$ in (33) should also represent the population mean TAC and BrAC response to the oral dosing described in Section 5.1. Thus, we validate the population model by comparing the averaged TAC and BrAC signals across the 267 samples in our dataset to the quantities $\{y_k^N\}$ and $\{z_k^N\}$, respectively, in the finite dimensional approximating population model (33) with the fit distributions of the parameters.

In the left panel of Figure 6, we have plotted these sample means along with the TAC and BrAC output, $\{y_k^N\}$ and $\{z_k^N\}$, respectively, from our finite dimensional approximating population model (33) with q_1, q_2, and q_3 random with the fit distributions shown in Figure 5. The $\{y_k^N\}$ curve is referred to as ETAC in the plot legend while the $\{z_k^N\}$ curve is referred to as EBrAC in the plot legend.

The error is given in the upper table in Table 2 in which the columns are (1) BrAC relative L_1 error, (2) TAC relative L_1 error, (3) peak BrAC relative error, (4) peak TAC relative error, (5) time of peak BrAC error (h), (6) time of peak TAC error (h), (7) area under BrAC curve relative error, and (8) area under TAC curve relative error.

TABLE 2 Validation results for the population model (upper table), the linear state estimator (center table), and the nonlinear state estimator (lower table).

1	**2**	**3**	**4**	**5**	**6**	**7**	**8**
0.16	0.12	0.02	0.11	0.68	0.08	0.11	0.04
1	**2**	**3**	**4**	**5**	**6**	**7**	**8**
0.18	0.14	0.02	0.08	0.68	0.07	0.11	0.01
1	**2**	**3**	**4**	**5**	**6**	**7**	**8**
0.18	0.12	0.02	0.11	0.68	0.08	0.12	0.03

5.4 | Validation of the state estimator

To validate our population state estimators we again used the Luczak human subject BrAC/TAC data described in Section 5.1 and tested how well both our linear-and nonlinear-, and both ourfinite time horizon-and steady state Kalman-population model-based state estimators described earlier could track the population means of the BrAC and TAC data. The results presented here are for the finite time horizon observer; the results for the steady state estimator were virtually identical.

Our validation results for the linear estimator are given in the center panel of Figure 6 and the center table in Table 2. In the center panel of Figure 6, we again plot the averaged TAC and BrAC signals across the 267 samples in our dataset along with the finite dimensional approximating estimators for the linear population model's output and controlled variables, $\{y_k\}$ and $\{z_k\}$, $\{\tilde{y}_k^N\}$ and $\{\tilde{z}_k^N\}$, where $\tilde{y}_k^N = \hat{C}^N \tilde{x}_k^N$ and $\tilde{z}_k^N = \hat{D}^N \tilde{x}_k^N$, with the finite dimensional approximating estimated state of the population model given by (37). In the center table of Table 2, the columns are (1) BrAC relative L_1 error, (2) TAC relative L_1 error, (3) peak BrAC relative error, (4) peak TAC relative error, (5) time of peak BrAC error (h), (6) time of peak TAC error (h), (7) area under BrAC curve relative error, and (8) area under TAC curve relative error. These results were obtained with the noise standard deviations taken to be $\sigma_1 = 0.005$, $\sigma_2 = 0.005$, and $\sigma = 0.1$. The model was linearized about the equilibrium solution corresponding to $\hat{v}(t) = \hat{v}_0 = \hat{v}^0 = 0.01$. The resulting equilibrium solution is given $\hat{x}_0(\eta) = 0.001\eta + 0.009$, $\hat{w}_0 = 0.009$, $\hat{u}_0 = 0.03$, and $\hat{y}_0 = 0.009$.

Our validation results for the nonlinear estimator are given in the right panel of Figure 6 and the lower table in Table 2. In the right panel of Figure 6, we again plot the averaged TAC and BrAC signals across the 267 samples in our dataset along with the finite dimensional approximating estimators, $\{\tilde{y}_k^N\}$ and $\{\tilde{z}_k^N\}$, for the output and controlled variables, $\{y_k\}$ and $\{z_k\}$, given in (20) for the nonlinear population model, (19), where $\tilde{y}_k^N = \hat{C}^N \tilde{x}_k^N$ and $\tilde{z}_k^N = \hat{D}^N \tilde{x}_k^N$, with the finite dimensional approximating estimated state $\tilde{x}_k^N$ of the nonlinear population model given by (31), (32) with $\tilde{x}_k$, $\tilde{u}_k$ $\hat{\mathcal{A}}$, $\hat{\mathcal{B}}$, and $\hat{\mathcal{C}}$ replaced by $\tilde{x}_k^N$, $\tilde{u}_k^N$, $\hat{\mathcal{A}}^N$, $\hat{\mathcal{B}}^N$, and $\hat{\mathcal{C}}^N$, respectively. In the lower table of Table 2, the columns are once again (1) BrAC relative L_1 error, (2) TAC relative L_1 error, (3) peak BrAC relative error, (4) peak TAC relative error, (5) time of peak BrAC error (h), (6) time of peak TAC error (h), (7) area under BrAC curve relative error, and (8) area under TAC curve relative error. These results were obtained with the noise standard deviations $\sigma_1 = 0.005$, $\sigma_2 = 0.005$ and $\sigma = 0.05$.

6 | SIMULATING CONTROLLED INTRAVENOUS ALCOHOL INFUSION

In this section, we demonstrate the efficacy of our approach by simulating the TAC biosensor-based output feedback control first of intravenously infused alcohol clamping experiments and then of the intravenous treatment of alcohol withdrawal symptoms. We note that in all of the simulations in this section we designed compensators (both the controller and observer) using both the time dependent solutions to the approximating finite time horizon Riccati difference equations and the steady state solutions to the infinite time horizon algebraic Riccati equations. We observed essentially no difference in the resulting closed loop control or state trajectories. In the case of the steady state control and observer algebraic Riccati equations, (36) and (39), respectively, we used either the routine dlqr or idare, both from the Matlab Control Toolbox. These routines are based on either an eigenvale/eigenvector[59] or Schur vector decomposition[60] of the

symplectic matrix (the discrete time analog of the Hamiltonian matrix in the continuous time case). The strong open loop stability of the systems seems to yield very well-conditioned Riccati equations, even when the discretization levels were chosen quite large. Consequently, we do not believe that more sophisticated Riccati solvers yielding enhanced numerical stability by avoiding the inversion of ill-conditioned matrices (see, e.g., Reference 61) are required for the problems we consider here.

Clamping studies are common in the pharmacokinetic literature and offer a number of benefits when investigating the body's ability to tolerate a particular drug, for example, alcohol. The aim of alcohol clamping is to have the subject reach a specified level of intoxication and to then remain at that level for an extended period of time. This allows researchers to investigate, for example, the phenomenon known as *decreased effect with prolonged exposure* (see References 3 and 4). In addition, *clamping*[3,4] is used by alcohol researchers to study alcohol metabolism, acute tolerance, and alcohol elimination, including individual differences based on sex, ethnicity, body composition, hormone levels, recent drinking history, and alcohol metabolizing gene variations[3,62-67] as well as episode-level variations due to factors such as stomach contents, liver blood flow, and hormone levels.[4,67,68] The technique enables researchers to bypass the oral consumption of alcohol and stomach/gut/liver metabolism and instead begin studies with alcohol directly administered into the blood, thereby eliminating confounding variability in alcohol absorption processes due to person- and episode-level factors.[4] In this way, it becomes possible to study factors specifically related to alcohol elimination rates.

When ethanol is intravenously infused, the typical means for regulating BAC is to measure BrAC and to then follow one of two protocols: (1) following a precalculated oral dosing to bring the BrAC up to the desired level, which typically takes approximately 40 min, the researcher would have the study participant periodically breathe into a breath analyzer, and based on the reading, manually adjust the intravenous flow of ethanol in the hope of maintaining BrAC at the constant target level, or alternatively, (2) use a "quick clamping" method that has been developed in which a sophisticated pharmacokinetic model with participant-dependent parameters is used to calculate an appropriate a-priori intravenous dose that will rapidly bring the participant's BrAC up to the target level (typically taking ∼20 min) and then attempt to manually maintain it at that level for an extended period of time.

The control objective is to clamp the subject's BAC at a target level of 0.06 g/dL by intravenously infusing a 6% V/V solution of ethanol. Our compensator was designed using the population model and corresponding state estimator based on either the nonlinear model given in (2) or its linearization, given in (3) with the parameters fit to the human subject data described in Sections 5.3 and 5.4. The linearization was about the plant steady state solution, $\hat{x}_0$, $\hat{w}_0$, and $\hat{u}_0$, corresponding to the target BAC level $\hat{v}^0 = 0.06$. As described in Sections 2.2 and 5, $\hat{w}_0$, and $\hat{u}_0$ which are required to implement the controller, as well as the loading dose, $\hat{u}^0$, can be calculated for the subject independently of the plant model with unknown parameters[48] either empirically or based on a statistical regression model with predictor variables from among available covariates such as sex, height, weight, and so forth.

We designed linear compensators based on the linearized model and both a linear and nonlinear estimator, and we designed nonlinear compensators using the nonlinear model and the nonlinear estimator. We set $T = 15$ or 30 h and assumed a noise level of approximately 10%, setting $\sigma_1 = \sigma_2 = \sigma = 0.006$, both in our design and in the simulation. In the performance index we set $\rho = \nu = 5.0$ and $\hat{r} = 0.05$. If the control penalty is set too low, the alcohol infusion rate can become negative or exceed what would be considered safe for an experiment or treatment involving human subjects. We simulated the plant with $n = 32$ and the compensator with $n = 4$ and $m_i = 4$, $i = 1, 2, 3$ resulting in a compensator of dimension 320. The sampling rate was 1/60 Hz or $\tau = 0.0167$ h (i.e., 1 sample per minute).

Since our design is based on a population model, it is most appropriate to present our results statistically. We simulated our compensator for each of the subjects in the combined male and female cohort ($N = 267$) described in Section 5.1. To simulate the plant we used the individual model given in (2) using the parameters obtained by fitting that model to that subject's BrAC and TAC data collected in the laboratory. The compensator was designed using the population model fit to the 95 of the cohort's individual parameters as described in Section 5.3. This is reasonable since it is assumed that in practice the compensator would be designed using a population model from a cohort, that based on appropriately selected covariates, includes the subject as a member but not necessarily part of the training set. We note that we also tested our approach on the male and female cohorts separately with the results being similar.

In the figures below, we plot simulation results for either the controlled BAC or the alcohol infusion rate (i.e., the control) for the entire merged cohort (i.e., male and female, $N = 267$). The target equilibrium BAC and mean target

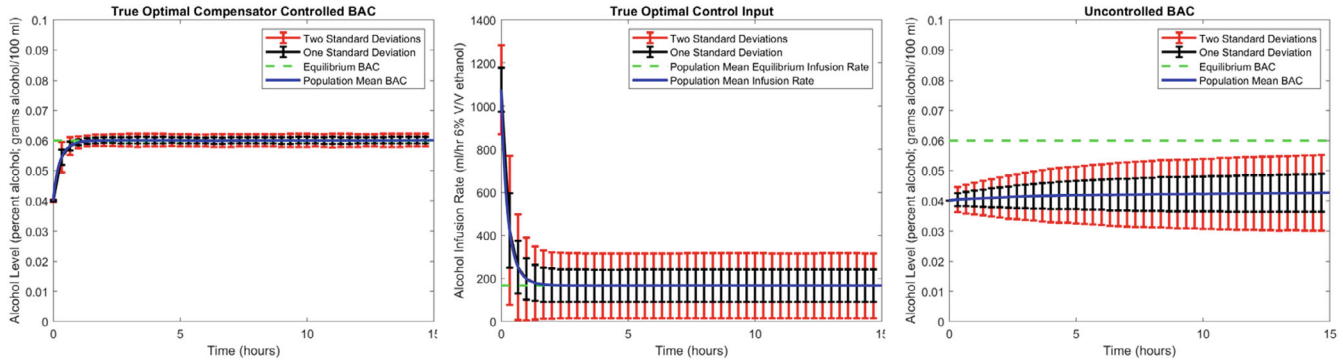

FIGURE 7 Left panel: Closed-loop BAC with optimal compensator based on known plant parameters; Center panel: intravenous ethanol infusion rate based on compensator designed using known plant parameters; Right panel: open-loop (maintenance dose only) BAC

infusion rate are plotted in green, the sample mean controlled BAC and sample mean alcohol infusion rate are plotted in blue (which by the law of large numbers, we would expect to be close to the respective population means), the black error bars are the point-wise sample standard deviations, and the red error bars are two sample standard deviations. Since our primary objective is regulation (or just returning to the target BAC after a short interruption, for example, to allow the subject to use the bathroom), for initial conditions, we assumed that the BAC level was 0.04 g/dL with the control objective being to bring the BAC level back up to the target level of 0.06 g/dL and to then maintain it at that level. We are primarily interested in regulation about steady state since the dose to initially bring the subject up to the target BAC level can be computed independently of the model using observable covariates such as sex, height, weight, total body water, and so forth.

As a basis for comparison, in the left and center panel of Figure 7, we plot, respectively, the controlled BAC and the corresponding intravenous infusion rate for the entire 267 member cohort but with the compensator designed using each plant's fit deterministic parameters (as described in Section 5.2). In other words, in this case, it was assumed that the plant (parameters) for each subject was known and rather than using the population model, the compensator was designed using the individual model (2) with parameter values fit using the subject's laboratory collected BrAC and TAC data; to wit, the same ones used to simulate the plant. The plant was simulated with $n = 32$ and the compensator was designed with $n = 4$. In the right panel of Figure 7, we have plotted uncontrolled (i.e., zero control) or open-loop BAC for the 267 subjects. In this case, the constant input or maintenance dose, $u_k = \hat{u}_0$. One can see from the plot, and standard analysis reveals, that the parameters for this cohort are such that the system will tend back to the target BAC, $\hat{v}^0$, but extremely slowly.

In Figure 8, we have plotted the results for the entire cohort obtained with a compensator designed using our approach based on the population model fit and validated in Section 5.3. The left panel is the compensator-controlled BAC and the center panel is the corresponding controller. To demonstrate the robustness of our design, during the simulation, we allowed all of the plant parameters to vary by as much as 20%, at random times during the simulation. The controlled BAC for one of these simulations is plotted in the right panel. It is clear that the results were not significantly different from those plotted in the left panel where the plant parameters remained fixed throughout the simulation. The corresponding controller for the simulation in the right panel was not significantly different than the controller plotted in the center panel when the plant parameters remained fixed.

In Figure 9, we have plotted the results of using a compensator designed based on the individual model, the same model as the plant, but with incorrect parameters. For each subject, the design parameters used were the parameters for a different subject in the cohort selected at random. The controlled BAC for one of these simulations is plotted in the left panel with the corresponding controller plotted in the center panel. The controlled BAC for another less extreme simulation of this type is plotted in the right panel.

In the left panel of Figure 10, we have plotted the controlled BAC that resulted from an individual model-based compensator designed using the mean values for all three of the random parameters. The plot in the center panel is the controlled BAC that resulted from using a compensator designed using our approach but with the nonlinear controller and the nonlinear observer given by (31) and (32). The plot in the right panel is the nonlinear controller (31) that produced the controlled BAC plotted in the center panel.

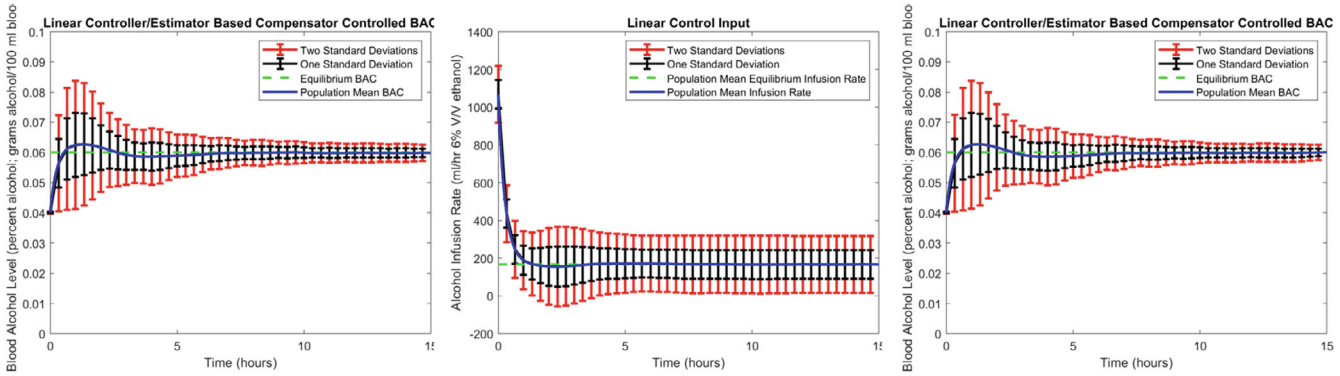

FIGURE 8 Left panel: population model based compensator controlled BAC; Center panel: corresponding controller or ethanol infusion rate; Right panel: controlled BAC when plant parameters vary by a random amount up to 20% at random times

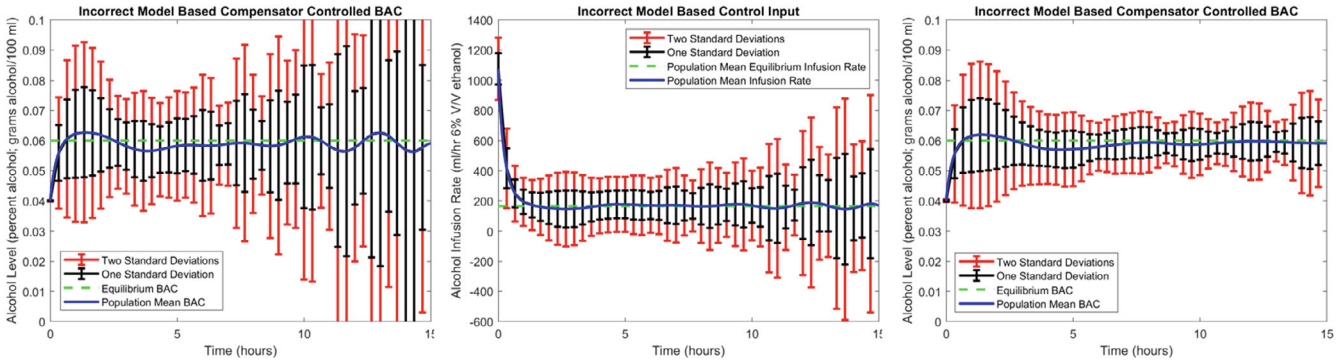

FIGURE 9 Left panel: Controlled BAC resulting from individual model-based compensators but designed using parameters other than the plant's selected at random from the cohort; Center panel: the corresponding control inputs; Right panel: compensator controlled BAC for another simulation like the one shown in the left panel but with a different random selection of design parameters from the cohort

Alcohol withdrawal syndrome (AWS) can pose a challenge to clinicians when patients suffering from alcohol use disorder, or AUD, are undergoing inpatient treatment, in particular, in the emergency department, the ICU, and the burn unit, and when they are having surgery. According to the American Psychiatric Association's *Diagnostic and Statistical Manual of Mental Disorders*,[69] symptoms of AWS may include nausea/vomiting, tremors, intermittent and intense sweating, anxiety, agitation and irritability, tactile disturbances and hallucinations including itching, pins and needles, burning, and numbness, auditory disturbances such as extreme sensitivity to sound and hearing things that do not exist, visual disturbances such as sensitivity to light and illusions and mirages, headache, balance disturbances such as dizziness and spinning sensations, disorientation with respect to date, time, and location, rapid heartbeat, elevated blood pressure, insomnia, general confusion, and grand mal seizures. Prophylactic intravenous infusion of ethanol is an inpatient therapy or treatment used in hospitals for preventing and alleviating the symptoms of AWS in these patients (see References 1, 2, and 70-72).

A protocol for infusing prophylactic intravenous ethanol is described in Reference 70. When a patient with a history of AUD and/or AWS is admitted, a 10% alcohol drip at 0.4 ml/kg/h should be initiated. BAC should be measured at 6, 24, and 72 h after infusion is started. If BAC exceeds 80 mg/dl (0.08%), infusion should be halted for 2 h then decreased by 50%, and the patient should be monitored for symptoms of AWS. If symptoms of AWS are no longer present after 24 h, infusion should be decreased by 20% after 48 h, decreased further by 50% after 72 h, decreased further by 50% after 84 h, and then discontinued. If the patient develops symptoms of alcohol withdrawal, increase infusion by 50%. It is clear that a protocol involving feedback control of BAC together with monitoring by medical personnel has the potential to improve both patient care and efficiency.

We simulate the use of our compensator to autonomously effect protocols for infusing prophylactic intravenous ethanol. Without the benefit of a TAC sensor and output feedback control, the steps in such a protocol are specified in

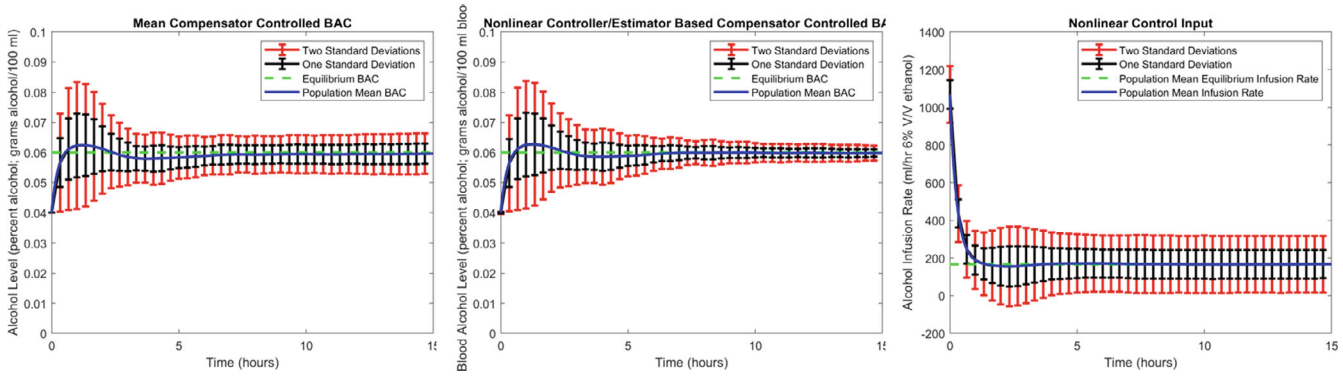

FIGURE 10 Left panel: Individual model based compensator controlled BAC using population means as parameters; Center panel: nonlinear control and estimator controlled BAC using our approach; Right panel: controller that produced BAC in center panel

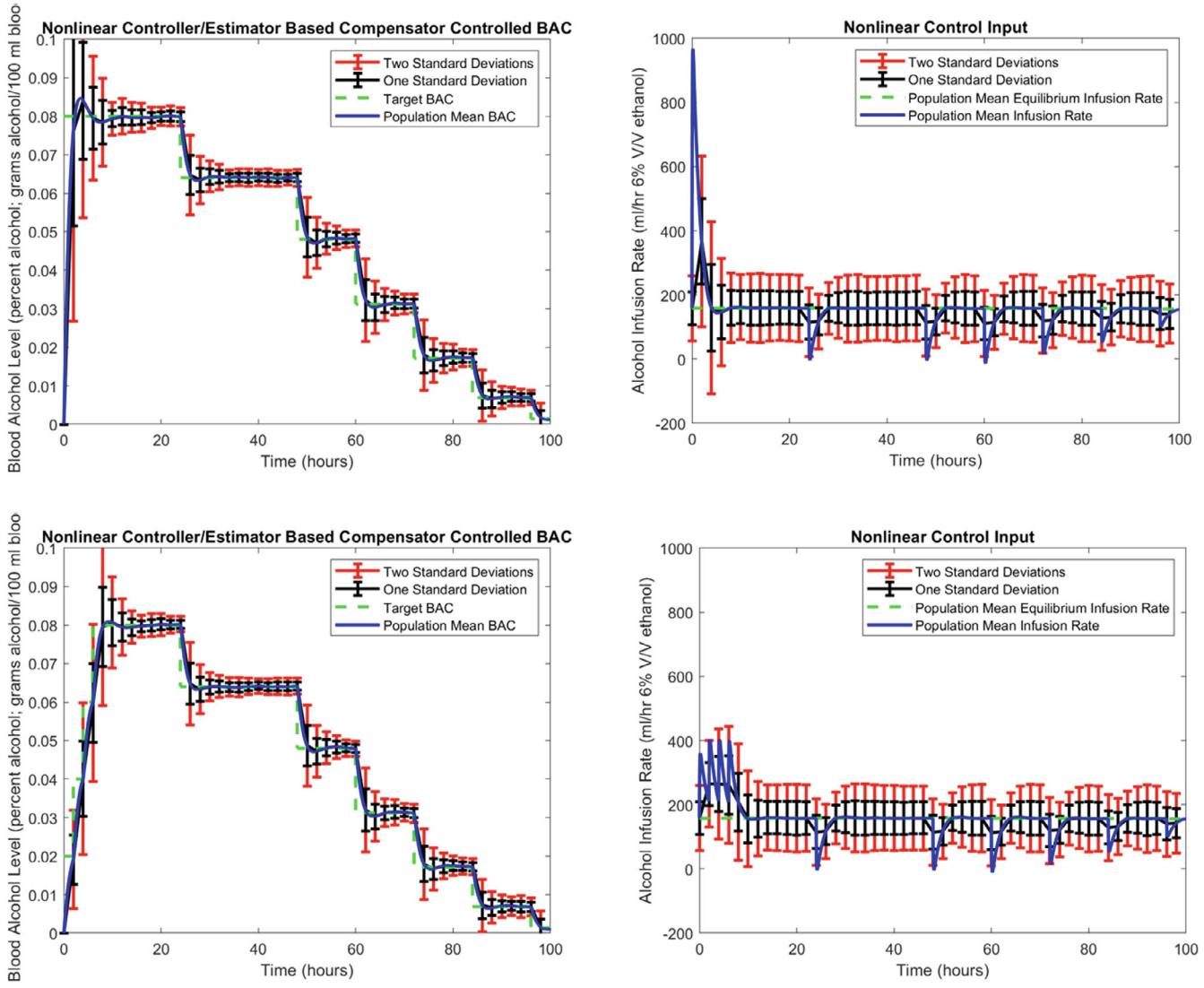

FIGURE 11 Upper left panel: Population model based compensator controlled protocol for infusing prophylactic intravenous ethanol over a four day treatment period; Upper right panel: the corresponding controller; Lower left panel: population model based compensator controlled protocol for infusing prophylactic intravenous ethanol over a four day treatment period with a more gradual ascending segment; Lower right panel: the corresponding controller

terms of reducing the ethanol infusion rate in a prespecified manner without regard to their effects other than what is observed. With the compensator and the TAC sensor, on the other hand, target BAC levels and time intervals are specified a-priori, then the controller forces the BAC to track them. The result of one such simulation is plotted in the upper two panels of Figure 11. The left panel is the controlled BAC and the right panel is the control. Note that in this simulation, we tested our compensator with an initial BAC level of 0.00 g/dL and an initial target BAC of $\hat{v}^0 = 0.08$. We used our nonlinear observer (32) and the nonlinear feedback controller (31) as given in Section 4.1.

Inspection of the controller in the upper right hand panel of Figure 11 reveals that specifying an initial target BAC of 0.08 yields an initial intravenous ethanol solution infusion rate of 1000 ml/h. Although this is for only a very short period time of 1 min, it is conceivable that such a high rate of intravenous infusion could compromise patient safety. The lower panels show the controlled BAC and corresponding control inputs when the target BAC is gradually increased to the ultimate target BAC of 0.08 over a longer period of time (6 h). In this case, the maximum infusion rate was approximately 400 ml/h.

7 | DISCUSSION AND CONCLUDING REMARKS

The simulation results plotted in Figures 8 and 10 in Section 6 demonstrate the efficacy of our population model-based compensator at regulating BAC about a target level. Comparing the left panel in Figure 8 and the center panel of Figure 10, we see that our linear and nonlinear compensators yield similar results. Comparing both of those plots with the left panel in Figure 10 we see that our population model designed compensators out-perform a compensator designed using the individual model but with the parameters taken to be the mean values of the plant parameters for the entire cohort. The right panel in Figure 8 demonstrates the robustness of our compensator design with respect to random variations in plant parameters of up to 20% occurring at random times during the simulation. This shows that our compensator is able to continue to regulate BAC level even if the physiological characteristics of the patient or subject, the calibration of the sensor, or the ambient conditions change as the study or treatment progresses. While the left panel in Figure 7 shows that a compensator designed using the individual model with the correct plant parameters performs extremely well, Figure 9 clearly shows that a compensator designed using the individual model but with parameters other than the plant's is a poor strategy and has the potential to lead to instability.

We note that it is possible to tune the performance of our compensator by adjusting the various design parameters, $\hat{r}$, ρ, and ν in the cost functional (22) or (23) or the noise variances σ_1^2, σ_2^2, or σ^2 in the Kalman observer. Performance could also be enhanced by stratifying the population into smaller cohorts of similar individuals based on covariates so as to reduce the variances of the random parameters, $q = [q_1, q_2, \ldots, q_8]$, appearing in the population model. Research on these ideas is on-going.

Beyond the rigorous mathematical theory upon which they are based, our numerical studies have demonstrated that our population model-based compensators perform well and that the finite-dimensional approximating compensators designed using our general approach for a plant of the form (18) converge. We also demonstrated that our compensators with fit distributions for the parameters perform well in both the case where the plant system parameters are fixed but unknown, and in the case where the plant parameters vary by random amounts at random times throughout the simulation.

One could ask if the closed-loop system consisting of the infinite-dimensional plant with either unknown or random parameters together with our finite-dimensional population model-based compensator could become unstable. Although we have seen no evidence of this, we continue to investigate this open question. In our other ongoing efforts, we are investigating the extension of the results presented here to LQG tracking for random abstract parabolic population models. This would permit intravenously infused alcohol studies where the target BAC level is replaced by a target BAC trajectory or reference signal. Finally, we anticipate that our population model-based tracking scheme will also yield an efficient and stable algorithm for the deconvolution of BAC or BrAC from a TAC signal in real time without the need to first calibrate the underlying model to the person, device, or environment.

Finally, we note that our results here demonstrate that TAC biosensor technology has potential utility well beyond simply serving as a replacement for the breathalyzer and as a novelty app in wearable consumer personal electronic devices. In addition, we have shown how linear quadratic control and estimation theory in infinite dimensional spaces (see, e.g., References 25, 26, 34, 40, 42, and 43) can be applied to plants with random parameters via population model-based designs. Our approach was based on a novel treatment of abstract random parabolic systems that results in a state space formulation in a Gelfand triple of Bochner spaces wherein the random parameters are effectively treated as additional

spatial variables.[35,36,40] In this way the LQ Kalman observer not only estimates the full state, but also effectively estimates the state's dependence on the uncertain parameters. While this framework for random parabolic systems was developed by others, and we have used it previously to develop estimation schemes that blindly deconvolve BAC or BrAC from TAC,[21-23] to the best of our knowledge, our effort here is the first time this approach has been applied in the context of control.

AUTHOR CONTRIBUTIONS

The clinical/experimental data used in this study was collected, organized, cleaned and made accessible by auhtors Saldich and Luczak. These authors also recruited the study participants and dealt with any IRB considerations and issues as they arose. The mathematical analysis, algoritm and computer code development, and computations were carried out by authors Yao and Rosen.

FUNDING INFORMATION

This work was supported in part by the National Institute on Alcohol Abuse and Alcoholism under Grants R21AA017711 and R01AA02636.

DATA AVAILABILITY STATEMENT

The data that support the findings of this study may be available on request from the corresponding author.

ORCID

I. Gary Rosen https://orcid.org/0000-0001-6801-9769

REFERENCES

1. Hansbrough JF, Zapata-Sirvent RL, Carroll WJ, Johnson R, Saunders CE, Barton CA. Administration of intravenous alcohol for prevention of withdrawal in alcoholic burn patients. *Am J Surg*. 1984;148(2):266-269.
2. Hodges B, Mazur JE. Intravenous ethanol for the treatment of alcohol withdrawal syndrome in critically ill patients. *Pharmacotherapy*. 2004;24(11):1578-1585.
3. O'Connor S, Morzorati S, Christian J, Li TK. Clamping breath alcohol concentration reduces experimental variance: application to the study of acute tolerance to alcohol and alcohol elimination rate. *Alcohol. Clin. Exp. Res*. 1998;22:202-210.
4. Ramchandani VA, O'Connor S, Neumark Y, Zimmermann US, Morzorati SL, de Wit H. The alcohol clamp: applications, challenges, and new directions - An RSA 2004 symposium summary. *Alcohol. Clin. Exp. Res*. 2006;30(1):155-164.
5. Nyman E, Palmlov A. The elimination of ethyl alcohol in sweat. *Acta Physiol*. 1936;74(2):155-159.
6. Swift RM. Transdermal measurement of alcohol consumption. *Addiction*. 1993;88(8):1037-1039.
7. Swift RM. Transdermal alcohol measurement for estimation of blood alcohol concentration. *Alcohol. Clin. Exp. Res*. 2000;24(4): 422-423.
8. Swift RM. Direct measurement of alcohol and its metabolites. *Addiction*. 2003;98:73-80.
9. Swift RM, Martin CS, Swette L, LaConti A, Kackley N. Studies on a wearable, electronic, transdermal alcohol sensor. *Alcohol. Clin. Exp. Res*. 1992;16(4):721-725.
10. Labianca DA. The chemical basis of the breathalyzer: a critical analysis. *J Chem Educ*. 1990;67:259-261.
11. Dumett MA, Rosen IG, Sabat J, et al. Deconvolving an estimate of breath measured blood alcohol concentration from biosensor collected transdermal ethanol data. *Appl Math Comput*. 2008;196(2):724-743.
12. Dai Z, Rosen IG, Wang C, Barnett N, Luczak SE. Using drinking data and pharmacokinetic modeling to calibrate transport model and blind deconvolution based data analysis software for transdermal alcohol biosensors. *Math Biosci Eng*. 2016;13:911-934.
13. Rosen IG, Luczak SE, Weiss J. Blind deconvolution for distributed parameter systems with unbounded input and output and determining blood alcohol concentration from transdermal biosensor data. *Appl Math Comput*. 2014;231:357-376.
14. Oszkinat C, Luczak S, Rosen IG. Uncertainty quantification in the estimation of blood alcohol concentration from Transdermal alcohol level using physics-informed neural networks. *IEEE Trans Neur Nets and Learn Sys*. 2022.
15. Oszkinat C, Luczak S, Rosen IG. A LSTM for the BRAC estimation of an abstract Parabolic system-based physics-informed long short-term memory network for estimating breath alcohol concentration from transdermal alcohol biosensor data. *Neural Comput Appl*. 2022.
16. Oszkinat C, Shao T, Wang C, et al. Obtaining blood and breath alcohol concentration from biosensor measured transdermal alcohol level: estimation and uncertainty quantification based on a covariate-dependent hidden Markov model; 2022.
17. Dougherty DM, Charles NE, Acheson JS, Furr RM, Hill-Kapturczak N. Comparing the detection of transdermal and breath alcohol concentrations during periods of alcohol consumption ranging from moderate drinking to binge drinking. *Exp Clin Psychopharmacol*. 2012;20:373-381.

18. Dougherty DM, Hill-Kapturczak N, Liang Y, et al. Use of continuous transdermal alcohol monitoring during a contingency management procedure to reduce excessive alcohol use. *Drug Alcohol Depend*. 2014;142:310-306.
19. Dougherty DM, Karns TE, Mullen J, et al. Transdermal alcohol concentration data collected during a contingency management program to reduce at-risk drinking. *Drug Alcohol Depend*. 2015;148:77-84.
20. Fairbairn CE, Kang D, Bosch N. Using machine learning for realtime BAC estimation from a new-generation transdermal biosensor in the laboratory. *Drug Alcohol Depend*. 2020;216:108205.
21. Sirlanci M, Rosen IG. Estimation of the distribution of random parameters in discrete time abstract parabolic systems with unbounded input and output: approximation and convergence. *Commun Appl Anal*. 2019;23(2):287-329.
22. Sirlanci M, Luczak SE, Fairbairn Ce E, et al. Estimating the distribution of random parameters in a diffusion equation forward model for a transdermal alcohol biosensor. *Automatica*. 2019;106:101-109.
23. Sirlanci M, Rosen IG, Luczak ES, Fairbairn CE, Bresin K, Kang D. Deconvolving the input to random abstract parabolic systems. A population model-based approach to estimating blood/breath alcohol concentration from transdermal alcohol biosensor data. *Inverse Probl*. 2018;34(12):125006.
24. Hawekotte K, Luczak SE, Rosen IG. Deconvolving breath alcohol concentration from biosensor measured transdermal alcohol level under uncertainty, a Bayesian approach. *Math Biosci Eng*. 2021;18(5):6739-6770.
25. Curtain R, Salamon D. Finite-dimensional compensators for infinite-dimensional systems with unbounded input operators. *SIAM J Control Optim*. 1986;24(4):797-816.
26. Pritchard AJ, Salamon D. The linear quadratic control problem for infinite dimensional systems with unbounded input and output operators. *SIAM J Contr Opt*. 1987;25(1):121-144.
27. Banks HT, Burns JA. Hereditary control problems: numerical methods based on averaging approximations. *SIAM J Control Optim*. 1976;16(2):169-208.
28. Banks HT, Kappel F. Spline approximations for functional differential equations. *J Differ Equ*. 1979;34(3):496-522.
29. Banks HT, Burns JA, Cliff EM. Parameter estimation and identification for systems with delays. *SIAM J Control Optim*. 1981;19(6):791-828.
30. Gibson JS. Linear-quadratic optimal control of hereditary differential systems: infinite dimensional Riccati equations and numerical approximations. *SIAM J Contr Opt*. 1983;21(1):95-139.
31. Rosen IG. A numerical scheme for the identification of hybrid systems describing the vibration of flexible beams with tip bodies. *J Math Anal Appl*. 1986;116:262-288.
32. Rosen IG. Spline-based Rayleigh-Ritz methods for the approximation of the natural modes of vibration for flexible beams with tip bodies. *Quart Appl Math*. 1986;XLIV:169-185.
33. Banks HT, Gates SS, Wang Y. The identification of a distributed parameter model for a flexible structure. *SIAM J Control Optim*. 1988;26:743-762.
34. Gibson JS, Rosen IG. Numerical approximation for the infinite-dimensional discrete-Time optimal linear-quadratic regulator problem. *SIAM J Control Optim*. 1988;26(2):428-451.
35. Gittelson CJ, Andreev R, Schwab C. Optimality of adaptive Galerkin methods for random parabolic partial differential equations. *J Comput Appl Math*. 2014;263:189-201.
36. Schwab C, Gittelson CJ. Sparse tensor discretizations of high-dimensional parametric and stochastic PDEs. *Acta Numer*. 2011;20:291-467.
37. Yao M, Luczak S, Rosen IG. Linear quadratic Gaussian control of random abstract parabolic systems. Proceedings of the 2021 IEEE Conference on Decision and Control (CDC); December 13-17, 2021; Austin, Texas, 2021.
38. Pazy A. *Semigroups of Linear Operators and Applications to Partial Differential Equations*. Springer; 1983.
39. Tanabe H. *Equations of Evolution*. Pitman; 1979.
40. Banks HT, Kunisch K. The linear regulator problem for parabolic systems. *SIAM J Cont Optim*. 1984;22(5):684-698.
41. Gibson JS. The Riccati integral equations for optimal control problems on Hilbert spaces. *SIAM J Cont Optim*. 1979;17(4):537-565.
42. Gibson JS, Rosen IG. Approximation of discrete-time LQG compensators for distributed systems with boundary input and unbounded measurement. *Automatica*. 1988;24(4):517-529.
43. Banks HT, Ito K. Approximation in LQR problems for infinite dimensional systems with unbounded input operators. *J Math Syst Est Control*. 1995;7(1):1-34.
44. Jones AW. Determination of liquid/air partition coefficients for dilute solutions of ethanol in water, whole blood, and plasma. *J Anal Toxicol*. 1983;7:193-197.
45. Mullen PW. The metabolism and pharmacokinetics of alcohol in man. *Forens Sci Sac*. 1977;17:49-55.
46. Balakrishnan AV. *Applied Functional Analysis*. 2nd ed. Springer-Verlag; 1981.
47. Tone C. εCentral limit theorems for Hilbert-space valued random fields satisfying a strong mixing conditionε, ALEA. *Lat Am J Probab Math Stat*. 2011;8:77-94.
48. Friel PN, Logan BK, O'Malley D, Baer JS. Development of dosing guidelines for reaching selected target breath alcohol concnetrations. *J Stud Alcohol*. 1999;60(4):555-565.
49. Watson PE, Watson ID, Batt RD. Total body water volumes for adult males and females estimated from simple anthropometric measurements. *Am J Clin Nutr*. 1980;33:27-39.
50. Banks HT, Flores KB, Rosen IG, Rutter EM, Sirlanci M, Thompson WC. The Prohorov metric framework and aggregate data inverse problems for random PDEs. *Commun Appl Anal*. 2018;22(3):415-446.
51. Li S, Luczak SE, Rosen IG. Identifying drinking patterns based on transdermal alcohol biosensor data and a random semi-linear hybrid partial and ordinary differential equation model for the metabolism and transdermal transport of ethanol. in preparation.

52. Banks HT, Ito K. A unified framework for approximation in inverse problems for distributed parameter systems. NASA Technical report. NASA-CR-181621, January 1988; Hampton, VA.
53. Lee KY, Chow S, Barr RO. On the control of discrete-Ttime distributed parameter systems. *SIAM J Control Optim*. 1972;10(2):361-376.
54. Kwakernaak H, Sivan R. *Linear Optimal Control Systems*. John Wiley; 1972.
55. Watson PE, Watson ID, Batt RD. Prediction of blood alcohol concentrations in human subjects: updating the Widmark equation. *J Stud Alcohol*. 1981;42:547-556.
56. Chumlea WC, Guo SS, Zeller CM, et al. Total body water reference values and prediction equations for adults. *Clinical Nephrol-Epidemiol-Clin Trials*. 2001;59(6):2250-2258. doi:10.1046/j.1523‐1755.2001.00741.x
57. Levi AJ, Rosen IG. A novel formulation of the adjoint method in the optimal design of quantum electronic devices. *SIAM J Control Optim*. 2010;48(5):3191-3223.
58. Casella G, Berger RL. *Statistical Inference*. 2nd ed. Duxbury; 2002.
59. Potter JE. Matrix quadratic solutions. *J SIAM Appl Math*. 1966;14(3):496-501.
60. Laub AJ. A Schur method for solving algebraic Riccati equations. *IEEE Trans Automat Contr*. 1979;AC-24:913-921.
61. Van Dooren P. A generalized eigenvalue approach for solving Riccati equations. *SIAM J Sci Stat Comput*. 1981;2:121-135.
62. Hesselbrock V, Higuchi S, Soyka M. Recent developments in the genetics of alcohol-related phenotypes. *Alcohol Clin Exp Res*. 2005;29:1321-1324.
63. Kwo PY, Ramchandani VA, O'Connor S, et al. Gender differences in alcohol metabolism: relationship to liver volume and effect of adjusting for body mass. *Gastroenterologia*. 1998;115:1552-1557.
64. Li TK, Beard JD, Orr WE, et al. Variation in ethanol pharmacokinetics and perceived gender and ethnic differences in alcohol elimination. *Alcohol Clin Exp Res*. 2000;24:415-416.
65. Neumark YD, Friedlander Y, Durst R, et al. Alcohol dehydrogenase polymorphisms influence alcohol-elimination rates in a male Jewish population. *Alcohol Clin Exp Res*. 2004;28:10-14.
66. Ramchandani VA, Bosron WF, Li TK. Research advances in ethanol metabolism. *Pathol Biol*. 2001;49:676-682.
67. Ramchandani VA, Flury L, Morzorati SL, et al. Recent drinking history: association with family history of alcoholism and the acute response to alcohol during a 60 mg% clamp. *J Stud Alcohol*. 2002;63:734-744.
68. Ramchandani VA, Kwo PY, Li TK. Effect of food and food composition on alcohol elimination rates in healthy men and women. *J Clin Pharmacol*. 2001;41:1345-1350.
69. Bayard M, Mcintyre J, Hill K, Woodside J Jr. Alcohol withdrawal syndrome. *Am Fam Physician*. 2004;69(6):1443-1450.
70. Dillard R, Welch T, Abdul-Hamed S, Kesey J, Dissanaike S. Ethanol infusion for alcohol withdrawal prophylaxis does not cause intoxication. *SWRCCC*. 2016;4(16):11-18.
71. Dissanaike S, Halldorsson A, Frezza EE, Griswold J. An ethanol protocol to prevent alcohol withdrawal syndrome. *J Am Coll Surg*. 2006;203(2):186-191.
72. Weinberg JA, Magnotti LJ, Fischer PE, et al. Comparison of intravenous ethanol versus diazepam for alcohol withdrawal prophylaxis in the trauma ICU: results of a randomized trial. *J Trauma*. 2008;64(1):99-104.

How to cite this article: Yao M, Luczak SE, Saldich EB, Rosen IG. A population model-based linear-quadratic Gaussian compensator for the control of intravenously infused alcohol studies and withdrawal symptom prophylaxis using transdermal sensing. *Optim Control Appl Meth*. 2022;1-29. doi: 10.1002/oca.2934